RESEARCH ARTICLE
SOLID EARTH: GEODESY AND GRAVITY

*Earth and Planetary Physics*
*10*: 630–647, 2026
doi: 10.26464/epp2026058

# Performance evaluation of the cold atom gravimeter WAG-H5-2#2508

**Lei Bai[1,2], YuFei Han[3], PanWei Huang[4*], YiXin Wang[4], XinLin Zhang[5], Peng Sang[1,2], WeiMin Zhang[2], YuanDe Yang[6], XiaoWei Niu[1,2], and LeLin Xing[1,2*]**

[1]Wuhan National Observation and Research Station for Geodesy, Wuhan 430077, China;

[2]Innovation Academy for Precision Measurement Science and Technology, Chinese Academy of Sciences (CAS), Wuhan 430077, China;

[3]China Earthquake Networks Center, Beijing 100045, China;

[4]CAS Cold Atom Technology (Wuhan) Company Limited, Wuhan 430070, China;

[5]Institute of Seismology, China Earthquake Administration, Wuhan 430071, China;

[6]Chinese Antarctic Center of Surveying and Mapping, Wuhan University, Wuhan 430079, China

**Key Points:**

- Detailed data processing, scientific evaluation methods, and multiple performance assessments are comprehensively demonstrated.
- Relative gravity measurements were conducted at four different heights using two CG-6 gravimeters, and precise vertical gravity gradients were obtained through quadratic fitting.
- Two constrained least-squares adjustment solutions were implemented to derive the comparison reference values and degrees of equivalence for each instrument.

**Citation:** Bai, L., Han, Y. F., Huang, P. W., Wang, Y. X., Zhang, X. L., Sang, P., Zhang, W. M., Yang, Y. D., Niu, X. W., Xing, L. L. (2026). Performance evaluation of the cold atom gravimeter WAG-H5-2#2508. *Earth Planet. Phys.*, *10*(4), 630–647. http://doi.org/10.26464/epp2026058

**Abstract:** The WAG-H5-2 atom gravimeter is an upgraded version of the WAG-H5-1. Compared with previous work, a highly integrated and stable optical system has been developed for the new gravimeter, based on the principle of matter–wave interferometry. The Comparison of Absolute Gravimeters for the CMONOC (Crustal Movement Observation Network of China) project was organized by the China Earthquake Networks Center from January 30 to March 30, 2026, in Wuhan. Our atom gravimeter (WAG-H5-2#2508) was invited to participate in this comparison. Absolute gravity at the indicated four sites was measured as requested by the organizer. Comparison results showed that no significant deviation existed between the WAG-H5-2#2508 atom gravimeter and laser interferometry absolute gravimeters, with deviations all within –4.3 to 6.1 μGal (1 μGal = $10^{-8}$ m/s$^2$). The performance of our instrument in terms of sensitivity, precision, repeatability, stability, and accuracy were evaluated. The WAG-H5-2#2508 exhibited a short-term sensitivity of 16.2 μGal/Hz$^{1/2}$ and achieved an observation precision of ~1.0 μGal over 1000 s. The measurement precision was better than 0.4 μGal, based on one-day observation data. The repeatability was approximately 1.5 μGal. Long-term gravity monitoring over half a month at a sampling interval of 88 s showed that the residual was within 10 μGal. The deviation of 1.4 μGal during the comparison represents the accuracy of the instrument compared with several other gravimeters (FG5X, A10, and IGG-03B).

**Keywords:** atom gravimeter; absolute gravity measurements; precision; accuracy; Allan deviation

## 1. Introduction

Gravimetry allows the determination of gravity acceleration ($g$) at specific positions as well as the detection of gravity changes with time and at a given location. For high-precision demands, the $g$-value has to be defined very accurately (Xu GC, 2010). Geodetic and geophysical studies, such as resource exploration (Xue GQ et al., 2024), tectonic studies (Sun WK et al., 2009), geoid determination (Guo DM et al., 2023), and the establishment and maintenance of a gravity reference network consistent with the International Terrestrial Gravity Reference Frame (ITGRF; Sánchez et al., 2023), can benefit from the combination of relative and absolute gravimetry (hybrid gravimetry; Hinderer et al., 2016). High-precision absolute gravity measurements can be conducted to establish and improve international and national gravity reference networks (Li ZC et al., 2018) and calibrate relative gravimeters (Wang QY et al., 2018; Mu LS et al., 2019), achieving a consistent regional and global standard through datum definition in level and scale and providing essential calibration systems for relative gravimetry (Wang LS et al., 2014).

First author: L. Bai, bailei@apm.ac.cn
Correspondence to: P. W. Huang, huangpanwei@cascoldatom.com
L. L. Xing, llxing@apm.ac.cn
Received 29 APR 2026; Accepted 13 MAY 2026.
First Published online 18 JUN 2026.

Traditionally, laser interferometry absolute gravimeters based on the free-fall principle (such as the FG5X and A10) have been the mainstream equipment. The laser interferometer-based absolute gravimeters have limitations in continuous long-term gravity measurements because of the mechanical movement. Compared with the classical gravimeter, the atom gravimeter, or quantum gravimeter, uses laser-cooled atoms as the test mass. It has no mechanical movement; therefore, mechanical wear has been avoided completely, and this unique attribute brings the absolute gravimeter excellent long-term, uninterrupted output performance. Quantum gravimeters based on atom interferometers have developed rapidly over the past two decades (Fang J et al., 2024). Atomic gravimetry is characterized by drift-free, long-term stability and high precision, providing long-term continuous measurements, and thus a new absolute gravity measurement method. China has achieved long-term technical accumulation in the field of transportable atom gravimeters (Zhou MK et al., 2015; Wang SK et al., 2018; Xu AP et al., 2019; Xu YY et al., 2022; Li CY et al., 2023). The first-generation WAG-H5-1 atom gravimeter developed in the early stage has verified the practical potential of atomic interferometry gravity measurement (Huang PW et al., 2019). Accordingly, this work focuses on the upgraded second-generation transportable atom gravimeter WAG-H5-2. This instrument has inherited the core principle of atomic interferometry measurement from the first generation, thus achieving a good balance between integration density and high performance.

For a newly developed practical absolute gravimeter, conducting a standardized comparison with mature gravimeters is a necessary step to comprehensively verify its performance. From January to March 2026, the developed WAG-H5-2#2508 was invited to participate in the absolute gravimeter comparison organized by the Crustal Movement Observation Network of China (CMONOC) project in Wuhan, and the instrument completed the measurement task at four stations together with eight absolute gravimeters from multiple institutions. In this article, we first introduce the working principle and system design of the WAG-H5-2, then elaborate in detail on the measurement scheme and rigorous data processing procedure of this comparison (including quadratic polynomial fitting of the vertical gravity gradients [VGGs], unified observation epoch reduction using superconducting gravimeter observations, and two constrained least-squares adjustment solutions to obtain comparison reference values [CRVs] and degrees of equivalence [DoEs]). Finally, the actual measurement performance of WAG-H5-2#2508 is comprehensively evaluated from multiple dimensions, including accuracy, sensitivity, repeatability, and long-term stability, verifying the reliability and applicability of this instrument as a high-precision transportable atom gravimeter.

## 2. Principle, Design, and Setup of the WAG-H5-2

### 2.1 Working Principle

High-precision atom gravimeters operate on the principle of atom interferometry, where laser-cooled atoms serve as ideal test masses in free fall. The measurement cycle commences with the preparation of a cold atomic ensemble. Rubidium-85 atoms are first cooled and trapped in a three-dimensional magneto-optical trap (3D MOT) using the combination of counter-propagating cooling beams and a quadrupole magnetic field generated by anti-Helmholtz coils (Figure 1). This initial stage traps approximately $10^8$ atoms at a temperature near the Doppler cooling limit. To achieve the lower temperature requirement for further interference processing, polarization gradient cooling is subsequently applied; by increasing the detuning of the cooling lasers and ramping down their intensity, the atomic cloud is further cooled to approximately 3–4 μK. Following a short molasses phase, the atoms are launched vertically in an atomic fountain configuration by introducing a frequency offset $\Delta f$ between the upward- and downward-propagating cooling beams, achieving a typical launch velocity of approximately 3.0 m/s.

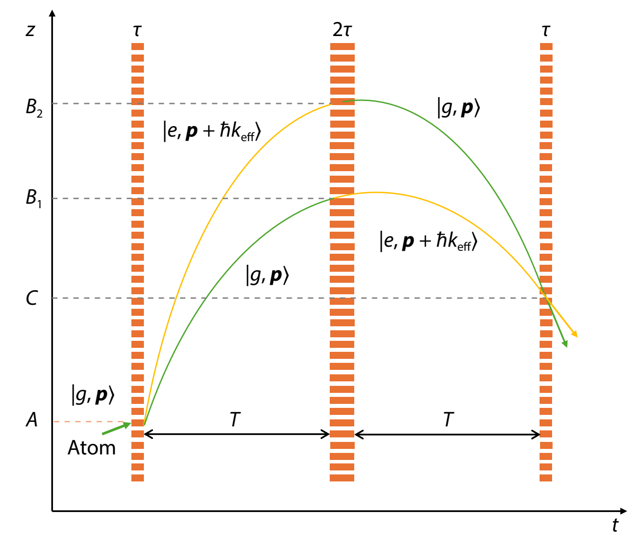


**Figure 1**. Working principle of a Mach-Zehnder type atom interferometer. $|g\rangle$ and $|e\rangle$ are the hyperfine levels on the groud electronic state of an atom, $|\boldsymbol{p}\rangle$ is the initial momentum state, $k_{\text{eff}}$ is the effective wave vector of an atom interferometer. Atoms are initially on the $|g, \boldsymbol{p}\rangle$ state, when they interact with a π/2 pulse, half of the atoms are excited to the $|e, \boldsymbol{p} + \hbar k_{\text{eff}}\rangle$ state, the other atoms are still on the $|g, \boldsymbol{p}\rangle$ state, then they are separated spatially. After a free evolution time of $T$, when atoms interact with a π pulse, the hyperfine states of the atoms invert and the momentum states exchange between atoms on different states. After another free evolution time of $T$, the separated atoms recombine spatially and a second π/2 pulse invert half of the atoms' states to create the interference pattern.

Prior to the interferometry sequence, the atomic sample undergoes state preparation to select a magnetically insensitive sublevel ($m_F = 0$) and to narrow the vertical velocity distribution. The core of the $g$-value measurement involves a Mach–Zehnder interferometer realized through stimulated Raman transitions between the $5^2S_{1/2}$ $|F = 3\rangle$ and $|F = 2\rangle$ hyperfine ground states. A sequence of three counter-propagating laser pulses, π/2, π, and π/2, separated by a free evolution time $T$ of 250 ms serves to split, redirect, and recombine the atomic wave packets. Because the atomic velocity changes under gravity, a time-dependent Doppler shift is induced. To maintain atom–light resonance, the frequency difference between the two Raman lasers is chirped at a rate of $\alpha = 2\pi\Delta f/T$. The resulting interference phase shift is given by

$$\Delta\Phi = (k_{\text{eff}} \cdot g - \alpha)T^2, \quad (1)$$

where $k_{eff} = k_1 - k_2$ is the effective wave vector of the counter-propagating Raman beams. The absolute value of gravitational acceleration is extracted by scanning the chirp rate $\alpha$ to determine the condition $\alpha_0 = k_{eff} \cdot g$, where the fringe phase becomes independent of the evolution time $T$.

### 2.2 Design and Setup

The WAG-H5-2 is a second-generation transportable quantum gravimeter developed by the CAS Cold Atom Co. Ltd. and was designed to balance ultimate measurement sensitivity with robustness. Architecturally, the instrument is partitioned into three highly integrated modules. The physical unit of the gravimeter is 0.50 × 0.23 × 1.34 m, including an active vibration isolation module and magnetic shielding. The optical and electronic units consist of four 3U (3-rack unit) chassis in total. The power consumption of the gravimeter is 480 W.

As shown in Figure 2, the physical unit includes a compact titanium vacuum chamber housing a 2D MOT for continuous atomic loading and a 3D MOT situated at the base of a 30 cm vertical fountain tube. The interference region is surrounded by mu-metal magnetic shielding, which attenuates ambient geomagnetic fluctuations. Active vibration isolation reduces the ambient ground noise contribution to approximately 4.5 μGal/Hz$^{1/2}$ via passive suppression and active damping by voice coil. A tip-tilt mirror stage compensates for the Coriolis force induced by the Earth's rotation, optimizing the fringe contrast and minimizing systematic bias.

The optical unit contributes considerably to the miniaturization of the system. It utilizes a single dual-channel fiber laser that serves as the seed for all required cooling, repumping, and Raman laser beams. The Raman laser phase is stabilized via an optical phase-locked loop. Instead of a traditional free-space bulk optical system, the unit utilizes an ultra-stable quartz-glass breadboard where miniature optical components and gradient-index lens couplers are bonded using a precision alignment technique. This monolithic integration minimizes optical misalignment resulting from thermal expansion or mechanical shock, ensuring that total optical power fluctuations remain below 5% even after 14,000 km of transportation (Zhu HR et al., 2024).

The electronic unit consolidates all control hardware, including a field-programmable gate array-based controller, low-noise current drivers, radio-frequency synthesizers, and detection circuits. A custom interface automates complex timing sequences with microsecond precision and performs real-time fringe fitting and $g$-value calculation.

Once the optical phase-locked loop and frequency locking systems are enabled, the atom fountain and interference fringes are optimized by adjusting the launching velocity and Raman pulse durations. A preliminary scan over different free evolution times $T$ identifies the zero-crossing chirp rate corresponding to the local absolute $g$-value. During continuous operation, the instrument cycles at around a 1 Hz repetition rate, acquiring a full fringe every 40 cycles. By interleaving the effective wave vector of the Raman lasers, some systematic effects are suppressed. The raw data are post-processed to correct the environmental perturbations, including Earth tides, polar motion, and barometric pressure variations. Furthermore, a systematic error analysis yields a total systematic uncertainty of 2.4 μGal, as shown in Table 1. In Table 1, systematic bias values listed as zero indicate that the corresponding systematic effects have been eliminated via calibration, correction, or compensation. Although the systematic bias is corrected to zero, the correction process is inevitably affected by instrument resolution, environmental fluctuations, device stability, and calibration repeatability. Therefore, uncertainty components are still evaluated for effects with zero systematic bias.

## 3. Comparison of Absolute Gravimeters

Before the comparison, all the participants approved the technical

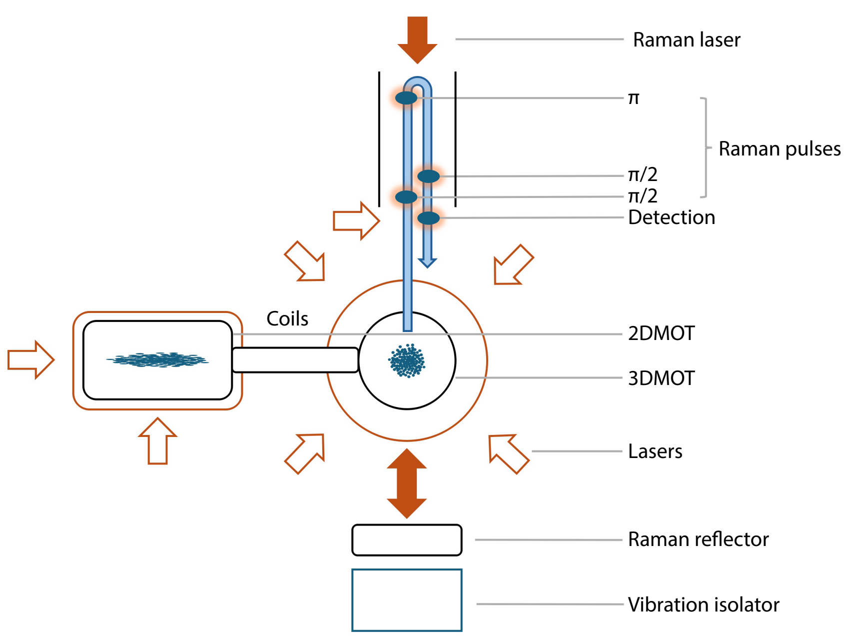


**Figure 2.** Physical unit of the WAG-H5-2.

**Table 1.** Typical systematic error budget of the WAG-H5-2.

| Systematic effect | Bias (μGal) | Uncertainty (μGal) |
|---|---|---|
| Laser frequency | −1.4 | 0.1 |
| Time standard | −12.9 | 0.8 |
| Verticality | 0 | 0.7 |
| Coriolis effect | 0 | 0.6 |
| Self-gravitation | −0.4 | 0.1 |
| Raman wavefronts | 0 | 2.0 |
| Zeeman effect | −0.3 | 0.6 |
| AC stark shift | 0 | 0.2 |
| Total | −15.0 | 2.4 |

protocol. The technical protocol includes the list of participants, a description of the comparison sites, the measurement strategy, a timetable of the measurements, and a standardized table to express the uncertainty of the gravimeters. It also includes tidal parameters and VGGs for the comparison sites. It specifies all the data processing as well as the result reports.

We give the list of participants who performed measurements during the comparison, the data (raw absolute gravity measurements and their uncertainties) submitted by the participants, and the results of the VGGs at the comparison sites. The measurement strategy and the method of data processing are presented comprehensively. Finally, the results of the data adjustment are presented, including the DoEs of the absolute gravimeters and the CRVs.

### 3.1 Participants

The performance of the WAG-H5-2 atom gravimeter was also evaluated in comparison with other absolute gravimeters during the annual comparison (since 2010) of the CMONOC project, which was held in Wuhan from January 30 to March 30 in 2026. The comparison was carried out in the urban environment of Wuhan city, China, which is approximately 30 km from downtown Wuhan and is far away from industry noise.

The list of participants is given in Table 2. In total, nine absolute gravimeters were compared. Except for the WAG-H5-2 absolute gravimeter, which is an atom gravimeter, all other instruments were conventional free-fall laser gravimeters. Among these instruments, the IGG-03B (Tian W et al., 2022) and WAG-H5-2 gravimeters are products manufactured by APM (Innovation Academy for Precision Measurement Science and Technology), CAS, and CAS Cold Atom Technology (Wuhan) Co. Ltd., respectively, whereas the others (FG5X and A10) are by Micro-g LaCoste Co. Ltd.

### 3.2 Site Description and Measurement Strategy

Gravity measurements were carried out at two stations in Wuhan, Hubei Province, China (Figure 3a): one was the Wuhan National Observation and Research Station for Geodesy (WNORSG), and the other was the Wuhan National Observation and Research Station for Gravitation and Earth Tide (WNORSGT). Both stations are located on Jiufeng Mountain and are less than 1.7 km apart, as shown in Figure 3b.

For the unified tidal correction model in the comparison, the tidal parameters (Sun HP et al., 2019) were provided to all the participants. Five gravity sites were used during the comparison. The station for WNORSG consists of three pillars with three gravity sites (JF009, JF018, and JF020), and that for WNORSGT consists of two pillars with two sites (JFCD0906 and JFCD0912), as shown in Figures 3c, 3d, and 4. Each gravimeter was planned to measure at four gravity sites. Thirty-six absolute gravity measurements were carried out by nine absolute gravimeters at five stations during the comparison, which are listed in Table 3. These were organized in two consecutive sessions (first session from January 30 to February 7; second session from March 5 to March 30).

The VGG has to be considered for two reasons. First, the average gradient is needed along the free-fall trajectory of an absolute gravimeter for a straightforward solution to the equation of motion. The second application of the gradient is the transfer of the $g$-value from the instrumental reference height (the distance between a benchmark and the effective position of free fall; Timmen, 2003) of each gravimeter to the comparison reference height (average of all instrumental reference heights), which can minimize the contribution of uncertainty resulting from transfer correction between two different heights (Jiang Z et al., 2012).

Because the sites at both Wuhan stations are close to mountain masses and located in underground spaces, the $g$-value exhibits a

**Table 2.** Participation of institutes and gravimeters.

| No. | Institution[a] | Gravimeter |
|---|---|---|
| 1 | Innovation Academy for Precision Measurement Science and Technology, CAS | A10#046 |
| 2 | Innovation Academy for Precision Measurement Science and Technology, CAS | FG5X#257 |
| 3 | The First Geodetic Surveying Brigade of the MNR | FG5X#260 |
| 4 | The First Geodetic Surveying Brigade of the MNR | A10#028 |
| 5 | CAS Cold Atom Technology (Wuhan) Co. Ltd. | WAG-H5-2#2508 |
| 6 | 61365 Troops of PLA | FG5X#264 |
| 7 | Institute of Seismology, China Earthquake Administration | FG5X#262 |
| 8 | Institute of Seismology, China Earthquake Administration | FG5X#255 |
| 9 | Innovation Academy for Precision Measurement Science and Technology, CAS | IGG-03B#005 |

[a]CAS, Chinese Academy of Sciences; MNR, Ministry of Natural Resources of the People's Republic of China; PLA, People's Liberation Army of China.

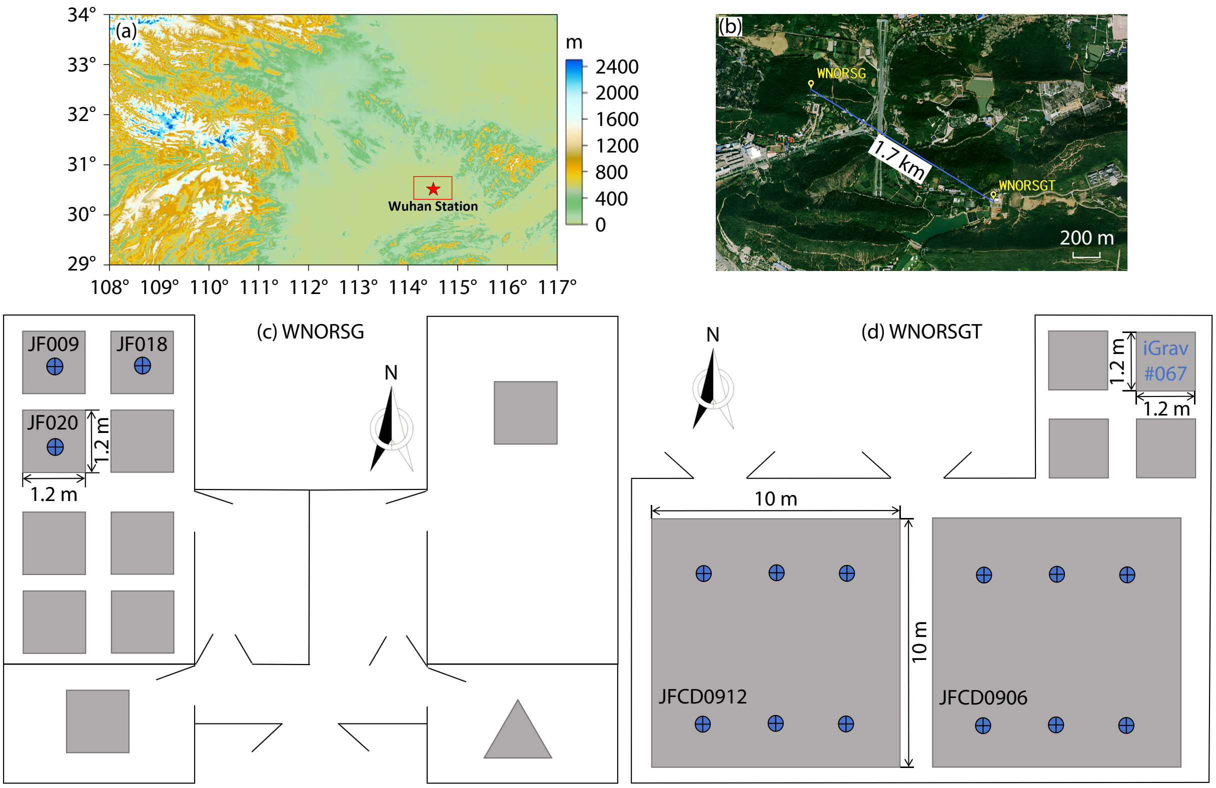


**Figure 3**. Two stations at Wuhan and sketch of the comparison sites. (a) Location and topographic relief of the Wuhan station. The red rectangle is the outline of (b). (b) Locations of the two stations from Google Earth. (c) Sketch of the sites at WNORSG, and (d) sketch of the sites at WNORSGT.

**Table 3.** Occupation of individual stations by gravimeters.

| Instrument | Station | | | | | |
|---|---|---|---|---|---|---|
| | JF009 | JF018 | JF020 | JFCD0906 | JFCD0912 | Total |
| WAG-H5-2#2508 | | √ | √ | √ | √ | 4 |
| IGG-03B#005 | √ | √ | | √ | √ | 4 |
| A10#028 | √ | √ | | √ | √ | 4 |
| A10#046 | √ | √ | √ | | √ | 4 |
| FG5X#255 | √ | √ | | √ | √ | 4 |
| FG5X#257 | √ | | √ | √ | √ | 4 |
| FG5X#260 | √ | √ | | √ | √ | 4 |
| FG5X#262 | √ | √ | | √ | √ | 4 |
| FG5X#264 | √ | √ | | √ | √ | 4 |
| Number of gravimeters occupying each station | 8 | 8 | 3 | 8 | 9 | |

nonlinear variation pattern with height. A quadratic polynomial model can better reflect the relationship between vertical gravity and height at each comparison site. Quadratic polynomial fitting was applied to approximate the $g$-value variation along the vertical distance above the ground benchmark (Jiang Z et al., 2012). The model of $g$ and the VGG at a specific height $h$ is (Jiang Z et al., 2012; Feng JY et al., 2022)

$$g(h) = a + b \cdot h + c \cdot h^2, \tag{2}$$

$$\mathrm{VGG}_{\mathrm{quadratic}} = b + 2 \cdot c \cdot h. \tag{3}$$

The second application of the gradient is the transfer of the $g$-value from the reference height of each gravimeter to the reference height defined for the comparison (comparison reference height). For the transfer correction, the height between $h_1$ and $h_2$ is used with the equation

$$\begin{gathered}\delta g(h_2 - h_1) = g(h_2) - g(h_1) = b \cdot (h_2 - h_1) + c \cdot \left(h_2^2 - h_1^2\right), \\ \sigma_{\delta g}^2 = (h_2 - h_1)^2 \cdot \sigma_b^2 + \left(h_2^2 - h_1^2\right)^2 \cdot \sigma_c^2 + 2 \cdot \left(h_2^2 - h_1^2\right) \cdot (h_2 - h_1) \cdot \sigma_{bc,}\end{gathered} \tag{4}$$

where $b$, $c$, $\sigma_b$, $\sigma_c$, $\sigma_{bc}$ are the first-order coefficient, the second-order coefficient, and their standard deviation and covariance.

To transfer the *g*-values from the instrumental height to a common reference height, the actual VGG above the benchmark should be used. The VGGs can be approximated by higher order polynomials. At the reference and comparison sites, it is recommended to determine VGGs from measurements of relative gravimeters carried out at least three levels above the benchmark, covering the range of typical instrumental reference heights (Wziontek et al., 2021). The reference height is instrument dependent: approximately 1.41 m, 0.72 m, 1.01 m, and 1.16 m for the FG5X, A10, IGG-03B, and WAG-H5-2, respectively. Vertical gravity gradients were calculated from gravity differences ($\delta g$) measured with Scintrex CG-6#052 and CG-6#056 relative gravimeters at four different vertical levels (0.20 m, ≈1.00 m, ≈1.30 m, and ≈1.50 m) at all the sites, as shown in Figure 5 and Table 4. The VGGs of linear fitting were also provided to all the participants, and the coefficients of the quadratic polynomial fitting at each station (shown in Table 5) could be used to transfer the *g*-values from the instrumental reference height to the comparison reference height of 1.10 m.

The raw absolute gravity measurements were presented by participants with corrections attributable to geophysical effects (tides, polar motion, and atmospheric mass redistribution) and instrumental effects (self-attraction, laser beam diffraction, and speed of light). The participants submitted the raw measurements (the final *g*-values with the combined uncertainties) for all the measured sites at the instrumental reference height.

A superconducting gravimeter (SG) iGrav#087 was installed on a neighboring pillar in WNORSGT, as shown in Figure 2. It was colocated, enabling side-by-side comparative measurements. The SG time series were obtained by applying corrections for tides, the atmosphere (−0.3 μGal/hPa), and polar motion with the same models as for the absolute gravity measurements (Van Camp et al., 2017). The gravity variations observed during the comparison (SG corrections) are shown in Figure 6. The SG corrections were obtained by averaging the SG observations over the same time window as each absolute gravity measurement session. According to the gravity variations, all the observations were related to 00:00 UTC (Coordinated Universal Time) on March 1, 2026, when the SG correction was zero.

The VGGs were used to transfer the *g*-values from the instrumental reference height to the comparison reference height of 1.10 m. The raw absolute gravity measurements were transferred to the *g*-values at 1.10 m above the mark of the gravity site by using the VGGs listed in Table 4. These *g*-values were then computed to the corresponding values at 00:00 UTC on March 1, 2026, by incorporating gravity variations during the comparison campaign (as shown in Figure 4) for the data adjustment. The related results are shown in Table 6.

The relative gravity observation was also performed using the CG-6#052 and CG-6#056 relative gravimeters, which had been calibrated in the Jiugongshan calibration line before measurement. A total of four round-trip closed measurements were conducted. The observation method involved traveling from site *a* to site *b* and then returning back to site *a*. The relative gravity observation data at each measured site were corrected for tides, atmospheric pressure, and drift, and the gravity difference ($\delta g$) between the two sites was the average value between the two relative gravity instrument observations. Because the height of the CG-6 gravimeter sensor after installation was approximately 0.20 m (Francis, 2021), the gravity difference between the two measured sites, obtained by using two relative gravimeters, was also approximately 0.20 m. The gravity differences at the height of 0.20 m could be transferred to 1.10 m, and then the gravity differences at the height of 1.10 m could be adjusted together with the *g*-values at the same height, thereby obtaining parameters such as the CRV of each site and the DoE of each absolute gravimeter. The $\delta g$s and

**Table 4.** Gravity difference ($\delta g$) with the standard deviation at the five sites.

| Site | $\sim h_0 – h_1$ (m) | $\delta g_{\sim h_0-h_1}$ (μGal) | $\sigma_{\delta g}$ (μGal) | $\sim h_0 – h_2$ (m) | $\delta g_{\sim h_0-h_2}$ (μGal) | $\sigma_{\delta g}$ (μGal) | $\sim h_0 – h_3$ (m) | $\delta g_{\sim h_0-h_1}$ (μGal) | $\sigma_{\delta g}$ (μGal) |
|---|---|---|---|---|---|---|---|---|---|
| JF009 | 0.975 | −212.8 | 0.5 | 1.306 | −298.8 | 1.0 | 1.500 | −346.8 | 0.4 |
| JF018 | 0.980 | −214.7 | 0.3 | 1.301 | −299.6 | 1.0 | 1.497 | −349.3 | 0.5 |
| JF020 | 0.977 | −227.7 | 1.4 | 1.306 | −320.7 | 1.1 | 1.498 | −374.1 | 0.9 |
| JFCD0906 | 1.004 | −226.1 | 0.2 | 1.360 | −325.7 | 0.2 | 1.509 | −367.2 | 0.3 |
| JFCD0912 | 1.001 | −220.8 | 0.5 | 1.361 | −318.1 | 0.4 | 1.504 | −357.6 | 0.4 |

**Table 5.** Linear fitting of VGGs with the standard deviation, and the first-order and second-order coefficients *b* and *c* with the standard deviations and their covariance at the five sites.

| Site | $VGG_{linear}$ (μGal·m$^{-1}$) | $\sigma_{VGG}$ (μGal·m$^{-1}$) | $b$ (μGal·m$^{-1}$) | $\sigma_b$ (μGal·m$^{-1}$) | $c$ (μGal·m$^{-2}$) | $\sigma_c$ (μGal·m$^{-2}$) | $\sigma_{bc}$ (μGal$^2$·m$^{-3}$) |
|---|---|---|---|---|---|---|---|
| JF009 | −267.8 | 3.60 | −292.58 | 2.24 | 15.08 | 1.34 | −2.94 |
| JF018 | −270.2 | 2.80 | −289.39 | 2.44 | 11.73 | 1.46 | −3.48 |
| JF020 | −288.8 | 2.20 | −303.95 | 0.14 | 9.27 | 0.08 | −0.01 |
| JFCD0906 | −280.6 | 0.32 | −282.91 | 0.24 | 1.39 | 0.14 | −0.03 |
| JFCD0912 | −274.1 | 0.76 | −278.72 | 3.10 | 2.78 | 1.84 | −5.60 |

**Figure 4**. Comparison photographs. Top left is at WNORSG, and top right is at WNORSGT. Bottom left is the superconducting gravimeter (SG) supported by Wuhan University, and bottom right shows relative measurements.

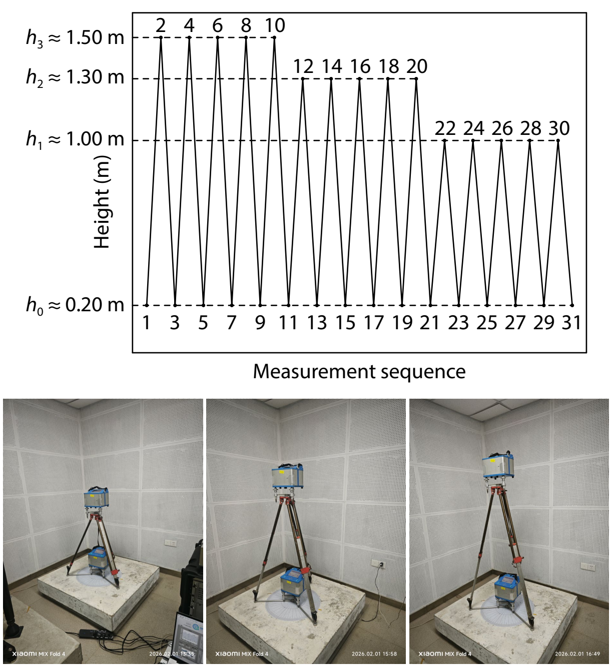


**Figure 5**. Vertical gravity gradient measurements at four different vertical levels. Top image shows the vertical gravity difference ($\delta g$) measurements at a site with 31 occupations; bottom images are measurement diagrams at the JF009 site.

their uncertainties at a height of 1.10 m were computed from the ones at 0.20 m according to Equation (4) and Table 5, as shown in Table 7.

The constant value $g_0$ has been subtracted from the gravity measurements. The term $u_{\mathrm{decl}}$ is the uncertainty declared by the participants, $u_{\mathrm{tran}}$ is the transfer uncertainty from the measurement or the instrumental reference height to the comparison reference height of 1.10 m when using VGG coefficients, and $u_{ik}$ is the uncertainty of the $g$-value measured by the $i$th gravimeter at the $k$th site, including the contribution of the uncertainty in the VGG transfer; $k$ is the coverage factor.

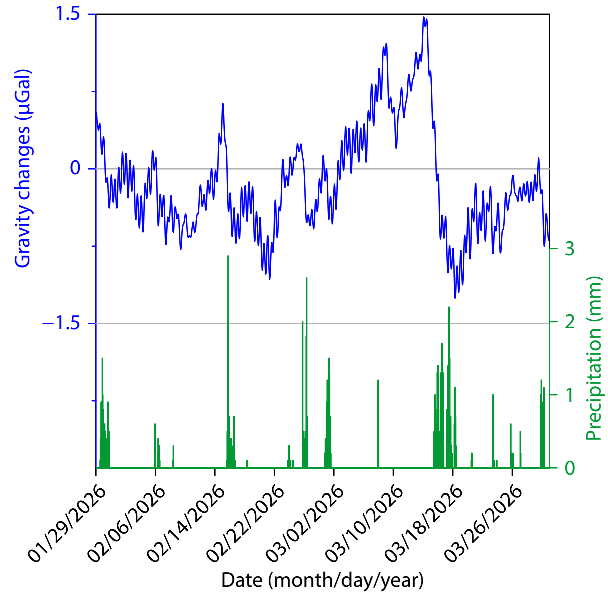


**Figure 6**. Gravity variation with tides, polar motion, the atmospheric effect correction, and precipitation during the comparison. Decimation filters were used to convert the raw data sampled at 1 s to 1 min; the residual gravity signal at 1 min was filtered to a 1-h interval, consistent with the time resolution of the absolute gravimeter. A meteorological instrument was installed, and the precipitation was recorded at 1-min intervals. As shown in the figure, the gravity decreased steeply during precipitation.

### 3.3 Method of Data Adjustment

There are two types of gravity observations: one is the $g$-value (Table 6), and the other is $\delta g$ (Table 7). The $g$-values cannot be directly compared because each gravimeter measured at only four of the five gravity sites. Two gravity data adjustment solutions are designed in this work: Solution A (only absolute gravity observations) and Solution B (a combination of absolute and relative gravity observations).

#### *3.3.1 Observation equation*

The absolute observation equation can be described as (Wu SQ, et al., 2021; Li CJ, et al., 2022)

$$g_{ik} = \hat{g}_k + \hat{\delta}_i + \varepsilon_{ik}, \tag{5}$$

where $i$ represents the gravimeter; $k$ represents the measured gravity site; $g_{ik}$ is the $g$-value transferred to the comparison reference height of 1.10 m at 00:00 UTC on March 1, 2026, which is the input to the absolute observation equation; $\hat{g}_k$ is the adjusted $g$-value, which is the output of the observation equation and is called the CRV at the height of 1.10 m above the mark of station $k$; $\hat{\delta}_i$ is the system bias of gravimeter $i$ and another output of the absolute observation equation, which is also the DoE of gravimeter $i$ and assumed to be a constant during the comparison; and $\varepsilon_{ik}$ is the random error.

**Table 6.** List of all the raw absolute gravity measurements from nine instruments corrected for geophysical effects, VGGs, and instrumental effects.

| Site | Time (UTC) Start time–end time | Instrument | Measurement height (m) | $g$ at measurement height (μGal) | $u_{decl}$ ($k$ = 1) (μGal) | VGG (μGal/cm) | δ$g$ transfer to 1.10 m (μGal) | $u_{tran}$ ($k$ = 1) (μGal) | $g$ at 1.10 m (μGal) | $u_{ik}$ ($k$ = 1) (μGal) | SG correctio ns (μGal) | $g$ after all corrections (μGal) |
|---|---|---|---|---|---|---|---|---|---|---|---|---|
| JF009 | 01-31-04:00–02-01-04:47 | A10#046 | 0.720 | −1584.9 | 10.5 | −2.708 | −100.75 | 0.2 | −1685.6 | 10.5 | 0.2 | −1685.4 |
| | 02-02-04:00–02-03-04:47 | FG5X#257 | 1.387 | −1763.4 | 1.8 | −2.507 | 73.20 | 0.4 | −1690.2 | 1.8 | 0.1 | −1690.1 |
| | 03-05-01:47–03-06-02:04 | FG5X#260 | 1.386 | −1773.4 | 1.8 | −2.508 | 72.95 | 0.3 | −1700.4 | 1.8 | −0.3 | −1700.7 |
| | 03-06-06:12–03-07-10:38 | A10#028 | 0.720 | −1592.0 | 10.5 | −2.708 | −100.75 | 0.2 | −1692.8 | 10.5 | −0.5 | −1693.3 |
| | 03-16-07:30–03-17-05:47 | FG5X#262 | 1.384 | −1768.9 | 1.8 | −2.508 | 72.45 | 0.3 | −1696.4 | 1.8 | 0.6 | −1695.8 |
| | 03-17-08:00–03-18-07:17 | FG5X#255 | 1.385 | −1766.8 | 1.8 | −2.508 | 72.70 | 0.3 | −1694.1 | 1.8 | 0.9 | −1693.2 |
| | 03-18-10:00–03-19-05:19 | IGG-03B#005 | 1.010 | −1666.0 | 5.0 | −2.621 | −23.47 | 0.1 | −1689.5 | 5.0 | 1.0 | −1688.5 |
| | 03-25-02:00–03-26-02:17 | FG5X#264 | 1.390 | −1769.2 | 1.8 | −2.506 | 73.96 | 0.4 | −1695.2 | 1.8 | 0.2 | −1695.0 |
| JF018 | 01-31-03:47–02-02-01:14 | WAG-H5-2#2508 | 1.163 | −1707.3 | 3.0 | −2.621 | 16.55 | 0.1 | −1690.8 | 3.0 | 0.1 | −1690.7 |
| | 02-02-04:00–02-03-04:47 | A10#046 | 0.720 | −1588.0 | 10.5 | −2.725 | −101.86 | 0.2 | −1689.9 | 10.5 | 0.1 | −1689.8 |
| | 03-05-04:46–03-06-05:15 | A10#028 | 0.720 | −1597.0 | 10.5 | −2.725 | −101.86 | 0.2 | −1698.9 | 10.5 | −0.3 | −1699.2 |
| | 03-06-08:07–03-07-08:24 | FG5X#260 | 1.388 | −1771.8 | 1.8 | −2.568 | 74.94 | 0.4 | −1696.9 | 1.8 | −0.5 | −1697.4 |
| | 03-16-08:00–03-17-07:17 | FG5X#255 | 1.385 | −1768.2 | 1.8 | −2.569 | 74.17 | 0.4 | −1694.0 | 1.8 | 0.9 | −1693.1 |
| | 03-18-08:00–03-19-01:17 | FG5X#262 | 1.386 | −1762.1 | 1.8 | −2.569 | 74.43 | 0.4 | −1687.7 | 1.8 | 1.0 | −1686.7 |
| | 03-19-07:00–03-20-06:19 | IGG-03B#005 | 1.010 | −1668.4 | 5.0 | −2.657 | −23.82 | 0.1 | −1692.2 | 5.0 | 0.7 | −1691.5 |
| | 03-26-03:30–03-26-15:47 | FG5X#264 | 1.391 | −1768.2 | 1.8 | −2.568 | 75.71 | 0.4 | −1692.5 | 1.8 | 0.2 | −1692.3 |
| JF020 | 01-30-00:00–01-31-00:47 | A10#046 | 0.720 | −1558.2 | 10.5 | −2.906 | −109.08 | 0.1 | −1667.3 | 10.5 | 0.1 | −1667.2 |
| | 01-31-04:00–02-01-04:47 | FG5X#257 | 1.383 | −1753.4 | 1.8 | −2.783 | 79.5 | 0.1 | −1673.9 | 1.8 | 0.2 | −1673.7 |
| | 02-02-03:30–02-03-05:00 | WAG-H5-2#2508 | 1.163 | −1689.4 | 3.0 | −2.824 | 17.83 | 0.1 | −1671.5 | 3.0 | 0.1 | −1671.4 |
| JFCD0906 | 03-10-02:08–03-11-02:25 | FG5X#260 | 1.384 | 1582.4 | 1.8 | −2.791 | 79.37 | 0.1 | 1661.8 | 1.8 | −0.5 | 1661.3 |
| | 03-12-01:00–03-13-01:17 | FG5X#257 | 1.385 | 1577.4 | 1.8 | −2.791 | 79.64 | 0.1 | 1657.0 | 1.8 | −0.9 | 1656.1 |
| | 03-13-03:26–03-14-03:55 | A10#028 | 0.720 | 1775.3 | 10.5 | −2.809 | −106.54 | 0.1 | 1668.8 | 10.5 | −1.2 | 1667.6 |
| | 03-17-04:00–03-18-04:19 | IGG-03B#005 | 1.010 | 1683.4 | 5.0 | −2.801 | −25.20 | 0.1 | 1658.2 | 5.0 | 0.9 | 1659.1 |
| | 03-19-04:00–03-20-06:17 | FG5X#262 | 1.383 | 1590.0 | 1.8 | −2.791 | 79.09 | 0.1 | 1669.1 | 1.8 | 0.8 | 1669.9 |
| | 03-20-08:30–03-21-06:47 | FG5X#255 | 1.382 | 1585.4 | 1.8 | −2.791 | 78.81 | 0.1 | 1664.2 | 1.8 | 0.4 | 1664.6 |
| | 03-22-02:50–03-23-02:16 | WAG-H5-2#2508 | 1.163 | 1647.6 | 3.0 | −2.797 | 17.62 | 0.1 | 1665.2 | 3.0 | 0.4 | 1665.6 |
| | 03-29-03:30–03-30-03:47 | FG5X#264 | 1.388 | 1587.1 | 1.8 | −2.790 | 80.48 | 0.1 | 1667.6 | 1.8 | 0.2 | 1667.8 |

**Continued from Table 6**

| Site | Time (UTC) Start time–end time | Instrument | Measurement height (m) | $g$ at measurement height (μGal) | $u_{decl}$ ($k$ = 1) (μGal) | VGG (μGal/cm) | $\delta g$ transfer to 1.10 m (μGal) | $u_{tran}$ ($k$ = 1) (μGal) | $g$ at 1.10 m (μGal) | $u_{ik}$ ($k$ = 1) (μGal) | SG corrections (μGal) | $g$ after all corrections (μGal) |
|---|---|---|---|---|---|---|---|---|---|---|---|---|
| | 03-08-02:33–03-09-04:50 | FG5X#260 | 1.386 | 1630.7 | 1.8 | −2.710 | 77.74 | 0.5 | 1708.4 | 1.9 | −1.0 | 1707.4 |
| | 03-10-12:00–03-11-12:17 | FG5X#257 | 1.388 | 1634.9 | 1.8 | −2.710 | 78.28 | 0.5 | 1713.2 | 1.9 | −0.5 | 1712.7 |
| | 03-12-02:22–03-13-02:51 | A10#028 | 0.720 | 1823.6 | 10.5 | −2.747 | −103.99 | 0.2 | 1719.6 | 10.5 | −0.9 | 1718.7 |
| | 03-13-07:26–03-14-08:43 | A10#046 | 0.720 | 1822.5 | 10.5 | −2.747 | −103.99 | 0.2 | 1718.5 | 10.5 | −1.2 | 1717.3 |
| JFCD0912 | 03-16-07:30–03-17-01:49 | IGG-03B#005 | 1.010 | 1737.7 | 5.0 | −2.731 | −24.56 | 0.1 | 1713.1 | 5.0 | 0.6 | 1713.7 |
| | 03-19-04:00–03-20-06:17 | FG5X#255 | 1.386 | 1624.9 | 1.8 | −2.710 | 77.74 | 0.5 | 1702.6 | 1.8 | 0.8 | 1703.4 |
| | 03-20-08:30–03-21-08:47 | FG5X#262 | 1.388 | 1634.6 | 1.8 | −2.710 | 78.28 | 0.5 | 1712.9 | 1.8 | 0.5 | 1713.4 |
| | 03-23-05:38–03-24-02:17 | WAG-H5-2#2508 | 1.163 | 1693.4 | 3.0 | −2.722 | 17.16 | 0.1 | 1710.6 | 3.0 | 0.6 | 1711.2 |
| | 03-28-02:00–03-29-02:17 | FG5X#264 | 1.392 | 1636.0 | 1.8 | −2.710 | 79.36 | 0.5 | 1715.4 | 1.9 | 0.2 | 1715.6 |

**Table 7.** Average gravity differences ($\delta g$s) and their standard deviations obtained by two CG-6 gravimeters, and the $\delta g$s at a height of 1.10 m and their uncertainties.

| Start site–end site | Average $\delta g$ of 0.20 m and its standard deviation (μGal) | | Correction of $g$-value at 0.20 m transferred to 1.10 m and its uncertainty ($k$ = 1) (μGal) | | | | Correction of $\delta g$ at 0.20 m transferred to 1.10 m and its uncertainty ($k$ = 1) (μGal) | | $\delta g$ of 1.10 m and its uncertainty ($k$ = 1) (μGal) | |
|---|---|---|---|---|---|---|---|---|---|---|
| | $\delta g$ (μGal) | $\sigma_{\delta g}$ (μGal) | Start site (μGal) | $u_{tran}$ (μGal) | End site (μGal) | $u_{tran}$ (μGal) | Correction of $\delta g$ (μGal) | $u_{tran}$ (μGal) | $\delta g$ (μGal) | $u_{\delta g}$ (μGal) |
| JF009–JF018 | 3.8 | 3.0 | 245.7 | 1.2 | 246.7 | 1.2 | −1.0 | 1.7 | 2.8 | 3.4 |
| JF018–JF020 | 33.8 | 2.7 | 246.7 | 1.2 | 262.7 | 0.1 | −16.0 | 1.2 | 17.8 | 3.0 |
| JF009–JFCD0912 | 3412.8 | 3.9 | 245.7 | 1.2 | 247.6 | 1.6 | −1.9 | 1.2 | 3410.9 | 4.1 |
| JFCD0912–JFCD0906 | −42.4 | 1.4 | 247.6 | 1.6 | 253.0 | 0.1 | −5.4 | 1.6 | −47.8 | 2.1 |

The relative observation equation is

$$\delta g_{ab} = \hat{g}_b - \hat{g}_a + \varepsilon_{ab}, \tag{6}$$

where $\delta g_{ab}$ is the $\delta g$ between site $a$ and $b$, $\hat{g}_a$ and $\hat{g}_b$ are the adjusted $g$-values of site $a$ and site $b$, and $\varepsilon_{ab}$ is the random error.

Assuming there are $m$ measurement sites and $n$ absolute gravimeters, there are a total of $t = m + n$ unknown parameters. Let $\hat{\boldsymbol{X}} = [\hat{g}_1\ \hat{g}_2 \cdots \hat{g}_m\ \hat{\delta}_1\ \hat{\delta}_2 \cdots \hat{\delta}_n]$, $\boldsymbol{G} = [g_{11}\ g_{12} \cdots g_{mn}]^{\mathrm{T}}$, and $\delta\boldsymbol{G} = [\delta g_{12}\ \delta g_{23} \cdots \delta g_{(m-1)m}]^{\mathrm{T}}$, the matrix expressions for the absolute observation Equation (5) and the relative observation Equation (6) are as follows:

$$\boldsymbol{V}_1 = \boldsymbol{A}_1\hat{\boldsymbol{X}} - \boldsymbol{G}, \tag{7}$$

$$\boldsymbol{V}_2 = \boldsymbol{A}_2\hat{\boldsymbol{X}} - \delta\boldsymbol{G}, \tag{8}$$

where $\boldsymbol{A}_1$ and $\boldsymbol{A}_2$ are the absolute observation design matrix and relative observation design matrix, respectively; and $\boldsymbol{V}_1$ and $\boldsymbol{V}_2$ are residual vectors.

*3.3.2 Constraint matrix and data weight matrix*

The weighted constraint is

$$\sum_i w_i\hat{\delta}_i = 0, \tag{9}$$

where $w_i$ is the weight assigned to the result of gravimeter $i$ with $\sum_i w_i = 1$, and $w_i$ is defined as ( Li CJ, et al., 2022)

$$w_i = \frac{1/u_i^2}{\sum_i 1/u_i^2}, \tag{10}$$

where $u_i$ is computed as the root mean square of $u_{ik}$, which is the standard uncertainty of gravimeter $i$ at station $k$.

The matrix expression is

$$\boldsymbol{V}_C = \boldsymbol{C}\hat{\boldsymbol{X}}, \tag{11}$$

where $\boldsymbol{V}_C$ is the constraint residual, where the constraint matrix $\boldsymbol{C}$ is a $1 \times t$ matrix used to solve the rank deficiency problem of the design matrix, with the form $\boldsymbol{C} = [0_{1\times m}\ w_1\ w_2 \cdots w_n]$. The data weight matrices are all diagonal matrices: for Solution A, the total matrix is $\boldsymbol{P}_{\text{total,A}} = \text{blkdiag}(\boldsymbol{P}_1, \boldsymbol{P}_C)$ where $\boldsymbol{P}_1 = \text{diag}(1/u_{ik}^2)$; for Solution B, the total matrix is $\boldsymbol{P}_{\text{total,B}} = \text{blkdiag}(\boldsymbol{P}_1, \boldsymbol{P}_2, \boldsymbol{P}_C)$ where $\boldsymbol{P}_2 = \text{diag}(1/u_{ab}^2)$, and $\boldsymbol{P}_C = \left[10^{12}\right]$ (a $1 \times 1$ diagonal matrix; the only diagonal element is $10^{12}$) is the constraint weight consistent in both solutions. Matrix $\boldsymbol{P}_C = \left[10^{12}\right]$ is an extremely large value, much larger than the observation weights. This means it is a strong constraint weight—assigning almost absolute weight to the constraint condition $\boldsymbol{CX} = 0$, forcing the constraint residual $\boldsymbol{V}_C$ to be close to 0, solving the rank deficiency of the design matrix, and ensuring the unique solution of unknown parameters.

*3.3.3 Adjustment solutions*

The matrix expression for the observation equation of Solution A is

$$\begin{bmatrix}\boldsymbol{V}_1\\ \boldsymbol{V}_C\end{bmatrix} = \begin{bmatrix}\boldsymbol{A}_1\\ \boldsymbol{C}\end{bmatrix}\hat{\boldsymbol{X}} - \begin{bmatrix}\boldsymbol{G}\\ 0\end{bmatrix}, \tag{12}$$

and for Solution B is

$$\begin{bmatrix}\boldsymbol{V}_1\\ \boldsymbol{V}_2\\ \boldsymbol{V}_C\end{bmatrix} = \begin{bmatrix}\boldsymbol{A}_1\\ \boldsymbol{A}_2\\ \boldsymbol{C}\end{bmatrix}\hat{\boldsymbol{X}} - \begin{bmatrix}\boldsymbol{G}\\ \delta\boldsymbol{G}\\ 0\end{bmatrix}. \tag{13}$$

Based on the unified model $\boldsymbol{V} = \boldsymbol{B}\hat{\boldsymbol{X}} - \boldsymbol{L}$ and the constrained total equation

$$\begin{bmatrix}\boldsymbol{V}\\ \boldsymbol{V}_C\end{bmatrix} = \begin{bmatrix}\boldsymbol{B}\\ \boldsymbol{C}\end{bmatrix}\hat{\boldsymbol{X}} - \begin{bmatrix}\boldsymbol{L}\\ 0\end{bmatrix}, \tag{14}$$

the parameter solution formula is unified as

$$\hat{\boldsymbol{X}} = \left(\boldsymbol{B}_{\text{total}}^{\mathrm{T}}\boldsymbol{P}_{\text{total}}\boldsymbol{B}_{\text{total}}\right)^{-1}\boldsymbol{B}_{\text{total}}^{\mathrm{T}}\boldsymbol{P}_{\text{total}}\boldsymbol{L}_{\text{total}}, \tag{15}$$

and for Solution A, $\boldsymbol{B}_{\text{total}} = \left[\boldsymbol{A}_1^{\mathrm{T}}\ \boldsymbol{C}^{\mathrm{T}}\right]^{\mathrm{T}}$, $\boldsymbol{L}_{\text{total}} = \left[\boldsymbol{G}^{\mathrm{T}}\ 0\right]^{\mathrm{T}}$, $\boldsymbol{P}_{\text{total}} = \boldsymbol{P}_{\text{total,A}}$; for Solution B, $\boldsymbol{B}_{\text{total}} = \left[\boldsymbol{A}_1^{\mathrm{T}}\ \boldsymbol{A}_2^{\mathrm{T}}\ \boldsymbol{C}^{\mathrm{T}}\right]^{\mathrm{T}}$, $\boldsymbol{L}_{\text{total}} = \left[\boldsymbol{G}^{\mathrm{T}}\ \delta\boldsymbol{G}^{\mathrm{T}}\ 0\right]^{\mathrm{T}}$, $\boldsymbol{P}_{\text{total}} = \boldsymbol{P}_{\text{total,B}}$.

The unit weight mean square error is

$$\hat{\sigma}_0 = \sqrt{\frac{\boldsymbol{V}_{\text{total}}^{\mathrm{T}}\boldsymbol{P}_{\text{total}}\boldsymbol{V}_{\text{total}}}{f}}, \tag{16}$$

where $f$ is the degrees of freedom, and

$$f = \text{total number of observations} + l - t.$$

The total number of observations refers to the total number of all observations; for Solution A, it is the number $g_{ik}$, and for Solution B, it is the sum of the number of $g_{ik}$ and $\delta g_{ab}$. In addition, $t = m + n$ is the total number of unknown parameters, and $l$ is the number of rank deficiency constraint conditions.

The standard uncertainty of the parameter is

$$\hat{\sigma}_{X_i} = \hat{\sigma}_0 \cdot \sqrt{\left(\boldsymbol{B}_{\text{total}}^{\mathrm{T}}\boldsymbol{P}_{\text{total}}\boldsymbol{B}_{\text{total}}\right)^{-1}(i, i)}. \tag{17}$$

*3.3.4 Gross error detection*

The compatibility index ($E_n$) value is an important index for evaluating the consistency between the observed value and the adjusted value; it is always used to judge the rationality of the adjustment result and the reliability of the observation data. Its core idea is to normalize the absolute difference between the observed value and the adjusted value by the expanded combined standard uncertainty under a specific confidence level, where the smaller the $E_n$ value, the better the consistency.

For gross error detection, a threshold of $3\sigma$ is more scientific and commonly adopted in measurement data processing. It corresponds to a 99.7% confidence level, which strictly follows the principle of small probability events and effectively avoids the false rejection of normal observations. By comparison, $2\sigma$ corresponds to a 95% confidence level, which is more suitable for expressing confidence intervals and measurement uncertainty rather than identifying gross errors (Wang SH, 2021). Therefore, a coverage factor $k = 3$ was adopted in this work. For absolute gravity observations, the $E_n$ value is defined by

$$E_{n_{ik}} = \frac{|g_{ik} - \hat{g}_k|}{k \cdot \sqrt{u_{ik}^2 + \hat{\sigma}_{g_k}^2}}, \tag{18}$$

where $\hat{\sigma}_{g_k}$ is the standard uncertainty of the final adjusted $g$-value $\hat{g}_k$, of the $k$th site. For the relative gravity observation, the $E_n$ value is defined by

$$E_{n_{ab}} = \frac{|\delta g_{ab} - \delta \hat{g}_{ab}|}{k \cdot \sqrt{u_{ab}^2 + \hat{\sigma}_{g_a}^2 + \hat{\sigma}_{g_b}^2}}, \tag{19}$$

where $\delta \hat{g}_{ab}$ is the difference in the final adjusted $g$-values of the $a$th and $b$th sites, and $\hat{\sigma}_{g_a}$ and $\hat{\sigma}_{g_b}$ are the standard uncertainties of the final adjusted $g$-values of the $a$th and $b$th sites, respectively.

### 3.4 Comparison Results

All the instrument measurements $g_{ik}$ were used based on the mathematical model described above. The values of $g_k$ and $\delta_i$ were calculated by using the weighted least-squares adjustment under the weighted condition for absolute observations.

The differences (DoEs, $g_{ik} - \hat{g}_k$) between the gravimeter $g$-values transferred to 1.10 m with all known corrections ($g_{ik}$) and the CRVs (the adjusted $g$-values at each station, $\hat{g}_k$) with their uncertainties for Solution A and Solution B are presented in Table 8. Those values were given by the square root of the sum of the square of the expanded uncertainty ($k$ = 3) of the $g$-value and of the CRVs. For Solution A, the DoEs of the nine gravimeters are −6.9 μGal (A10#028) and +9.2 (A10#046), and for Solution B, they are −7.0 μGal (A10#028) and +9.4 (A10#046). In other words, among the two solutions, the DoE of A10#028 is the most negative, whereas the DoE of A10#046 is the largest. This result mainly reflects the fact that the measurement uncertainty of the A10 gravimeter, which is approximately 10 μGal, is relatively reliable. The DoE of the WAG-H5-2#2508 gravimeter obtained from the two solutions ranges from 0.2 to 2.0 μGal, showing only a small difference compared with the CRVs, indicating that the measurement $g$-values of this gravimeter are highly accurate. This result is consistent with the instrument uncertainty of approximately 3.0 μGal given by the manufacturer.

An $E_n$ factor larger than 1.0 indicates that the measured $g$-value is incompatible at a 99.7% confidence level because their difference could not be converted by their uncertainties. This means that the measured $g$-value was corrupted or that the declared uncertainties were too small. The compatibility indexes $E_n$ of 36 measurements from the nine gravimeters, which are versus CRVs, are listed in Table 8. From the results, we also found that only two values of $E_n$ are greater than 1.0, at the JFCD0906 site and the JFCD0912 site, respectively, whereas values of the other gravimeters are all less than 1.0 at any site. Some studies have shown that the accuracy of the FG5X gravimeter is realistically approximately 3 μGal (Crossley et al., 2013). Because both stations are very “quiet” (have a low noise level), we can reach the conclusion that the uncertainty of the FG5X gravimeter may be greater than 2 μGal at a “quiet” site, given that the measurement is related not only to the instrument itself but also to the operator. Considering that only two values are greater than 1.0 and only slightly larger than 1.0 (1.2 and 1.1), we believe that these two $g$-values do not belong to outliers and that the declared uncertainties are slightly smaller. The final differences between $\delta g$ and $\delta \hat{g}$ and their uncertainties and $E_n$ are listed in Table 9. The results show that the differences are between −0.8 and 5.2 μGal and that all the compatibility indexes $E_n$ are less than 1.0.

The two main goals of the comparisons were to obtain the CRVs and their uncertainties, to determine whether the declared uncertainty of each instrument is accurate, and to acquire the DoEs of each instrument. The CRVs and their uncertainties for Solution A and Solution B at five sites are shown in Table 10. The accuracy of CRVs at three sites were found to be higher than 3.0 μGal, and the precision at the JF020 site was lower than the others. This is because the least number of gravimeters occupied site JF020 compared with the other three sites.

In addition, the difference in CRVs between the two solutions was very small, not exceeding 0.3 μGal, but the accuracy of the CRVs obtained by Solution B was higher than that of Solution A. Considering that the accuracy of the gravity data adjustment was approximately 3.0 μGal, these results indicate that the CRVs obtained by the two solutions have very good consistency.

The DoEs of all the gravimeters obtained by the two solutions are compared in Table 11 and Figure 7. The results show that all the gravimeters are in equivalence, with declared uncertainties at a 95% confidence level. Table 11 shows that the DoEs of all the gravimeters are between −4.3 and 6.1 μGal. Eight instruments have completely identical DoEs, except for the FG5X#257 gravimeter, which has a difference of 0.1 μGal.

The constant value $g_0$ has been subtracted from the CRVs. The uncertainty $U_i = 2\sigma$ ($\sigma$ is the standard deviation of the reference value from the data adjustment) is the expanded uncertainty at a 95% confidence level. All the $g$-values refer to 1.10 m above the marker.

## 4. Data Analysis

Four quantities are essential for assessing a gravimeter: accuracy, stability, repeatability, and continuous working capability. The accuracy is determined in Section 3. The stability and repeatability of the WAG-H5-2#2508 gravimeter were assessed using the observation data during comparison. Moreover, our instrument was transported from Wuhan to Tianjin over a long distance of approximately 1125 km. Continuous gravity monitoring was also carried out at the National Earthquake Metrology Station supported by the first Monitoring and Application Center, China Earthquake Administration, from February 1 to 16, 2024, in Tianjin (117.50°E, 40.08°N ) to verify the capability of long-term monitoring.

### 4.1 Short-Term Sensitivity

The sensitivity was assessed by calculating the Allan deviation of the gravity residual signal. During the comparison period, all gravimeters conducted continuous observations for more than 24 h at four of the five sites: JF009, JF018, JF020, JFCD0906, and JFCD0912. For the absolute gravimeters, measurement data were selected from two instruments, FG5X#257 and IGG03B#005, for the sensitivity calculation and to analyze their sensitivity and compare it with that of WAG-H5-2#2508. We chose the data at site JF018 for analysis because these three instruments all conducted observations at this site. The $g$-value at site JF018 was measured, and approximately 36 h of consecutive measurement data were obtained. For the relative gravimeter, in addition to selecting

**Table 8.** Comparison results of all the gravimeters.

| Gravimeter | Site | $g_{ik}$ after all corrections (μGal) | $U_{ik}$ ($k=1$) (μGal) | Solution A | | | | | Solution B | | | | |
|---|---|---|---|---|---|---|---|---|---|---|---|---|---|
| | | | | $\hat{g}_k$ (CRVs) (μGal) | $U_k$ ($k=1$) (μGal) | $g_{ik}-\hat{g}_k$ (μGal) | $U_{g_{ik}-\hat{g}_k}$ ($k=1$) (μGal) | $E_n$ | $\hat{g}_k$ (CRVs) (μGal) | $U_k$ ($k=1$) (μGal) | $g_{ik}-\hat{g}_k$ (μGal) | $U_{g_{ik}-\hat{g}_k}$ ($k=2$) (μGal) | $E_n$ |
| A10#046 | JF009 | −1685.4 | 10.5 | −1694.6 | 1.3 | 9.2 | 10.6 | 0.3 | −1694.8 | 1.2 | 9.4 | 10.6 | 0.3 |
| | JF018 | −1689.8 | 10.5 | −1692.3 | 1.5 | 2.5 | 10.6 | 0.1 | −1692.2 | 1.3 | 2.4 | 10.6 | 0.1 |
| | JF020 | −1667.2 | 10.5 | −1673.1 | 2.9 | 5.9 | 10.9 | 0.2 | −1673.4 | 2.3 | 6.2 | 10.8 | 0.2 |
| | JFCD0912 | 1717.3 | 10.5 | 1710.6 | 1.3 | 6.7 | 10.6 | 0.2 | 1710.9 | 1.2 | 6.4 | 10.6 | 0.2 |
| FG5X#257 | JF009 | −1690.1 | 1.8 | −1694.6 | 1.3 | 4.5 | 2.3 | 0.7 | −1694.8 | 1.2 | 4.7 | 2.2 | 0.7 |
| | JF020 | −1673.7 | 1.8 | −1673.1 | 2.9 | −0.6 | 3.4 | 0.1 | −1673.4 | 2.3 | −0.3 | 3.0 | 0.0 |
| | JFCD0906 | 1656.1 | 1.8 | 1664.0 | 1.3 | −7.9 | 2.2 | 1.2 | 1663.9 | 1.2 | −7.8 | 2.2 | 1.2 |
| | JFCD0912 | 1712.7 | 1.9 | 1710.6 | 1.3 | 2.1 | 2.3 | 0.3 | 1710.9 | 1.2 | 1.8 | 2.2 | 0.3 |
| FG5X#260 | JF009 | −1700.7 | 1.8 | −1694.6 | 1.3 | −6.1 | 2.3 | 0.9 | −1694.8 | 1.2 | −5.9 | 2.2 | 0.9 |
| | JF018 | −1697.4 | 1.8 | −1692.3 | 1.5 | −5.1 | 2.3 | 0.7 | −1692.2 | 1.3 | −5.2 | 2.2 | 0.8 |
| | JFCD0906 | 1661.3 | 1.8 | 1664.0 | 1.3 | −2.7 | 2.2 | 0.4 | 1663.9 | 1.2 | −2.6 | 2.2 | 0.4 |
| | JFCD0912 | 1707.4 | 1.9 | 1710.6 | 1.3 | −3.2 | 2.3 | 0.5 | 1710.9 | 1.2 | −3.5 | 2.2 | 0.5 |
| A10#028 | JF009 | −1693.3 | 10.5 | −1694.6 | 1.3 | 1.3 | 10.6 | 0.0 | −1694.8 | 1.2 | 1.5 | 10.6 | 0.0 |
| | JF018 | −1699.2 | 10.5 | −1692.3 | 1.5 | −6.9 | 10.6 | 0.2 | −1692.2 | 1.3 | −7.0 | 10.6 | 0.2 |
| | JFCD0906 | 1667.6 | 10.5 | 1664.0 | 1.3 | 3.6 | 10.6 | 0.1 | 1663.9 | 1.2 | 3.7 | 10.6 | 0.1 |
| | JFCD0912 | 1718.7 | 10.5 | 1710.6 | 1.3 | 8.1 | 10.6 | 0.3 | 1710.9 | 1.2 | 7.8 | 10.6 | 0.2 |
| FG5X#262 | JF009 | −1695.8 | 1.8 | −1694.6 | 1.3 | −1.2 | 2.25 | 0.2 | −1694.8 | 1.2 | −1.0 | 2.2 | 0.2 |
| | JF018 | −1686.7 | 1.8 | −1692.3 | 1.5 | 5.6 | 2.3 | 0.8 | −1692.2 | 1.3 | 5.5 | 2.2 | 0.8 |
| | JFCD0906 | 1669.9 | 1.8 | 1664.0 | 1.3 | 5.9 | 2.2 | 0.9 | 1663.9 | 1.2 | 6.0 | 2.2 | 0.9 |
| | JFCD0912 | 1713.4 | 1.8 | 1710.6 | 1.3 | 2.8 | 2.2 | 0.4 | 1710.9 | 1.2 | 2.5 | 2.2 | 0.4 |
| FG5X#255 | JF009 | −1693.2 | 1.8 | −1694.6 | 1.3 | 1.4 | 2.25 | 0.2 | −1694.8 | 1.2 | 1.6 | 2.2 | 0.2 |
| | JF018 | −1693.1 | 1.8 | −1692.3 | 1.5 | −0.8 | 2.3 | 0.1 | −1692.2 | 1.3 | −0.9 | 2.2 | 0.1 |
| | JFCD0906 | 1664.6 | 1.8 | 1664.0 | 1.3 | 0.6 | 2.2 | 0.1 | 1663.9 | 2.3 | 0.7 | 4.3 | 0.1 |
| | JFCD0912 | 1703.4 | 1.8 | 1710.6 | 1.3 | −7.2 | 2.2 | 1.1 | 1710.9 | 2.3 | −7.5 | 4.3 | 1.2 |
| IGG-03B#005 | JF009 | −1688.5 | 5 | −1694.6 | 1.3 | 6.1 | 5.15 | 0.4 | −1694.8 | 2.4 | 6.3 | 10.3 | 0.4 |
| | JF018 | −1691.5 | 5 | −1692.3 | 1.5 | 0.8 | 5.2 | 0.1 | −1692.2 | 2.5 | 0.7 | 10.3 | 0.0 |
| | JFCD0906 | 1659.1 | 5 | 1664.0 | 1.3 | −4.9 | 5.15 | 0.3 | 1663.9 | 2.3 | −4.8 | 10.3 | 0.3 |
| | JFCD0912 | 1713.7 | 5 | 1710.6 | 1.3 | 3.1 | 5.15 | 0.2 | 1710.9 | 2.3 | 2.8 | 10.3 | 0.2 |
| FG5X#264 | JF009 | −1695.0 | 1.8 | −1694.6 | 1.3 | −0.4 | 2.25 | 0.1 | −1694.8 | 2.4 | −0.2 | 4.3 | 0.0 |
| | JF018 | −1692.3 | 1.8 | −1692.3 | 1.5 | 0.0 | 2.3 | 0.0 | −1692.2 | 2.5 | −0.1 | 4.4 | 0.0 |
| | JFCD0906 | 1667.8 | 1.8 | 1664.0 | 1.3 | 3.8 | 2.2 | 0.6 | 1663.9 | 2.3 | 3.9 | 4.3 | 0.6 |
| | JFCD0912 | 1715.6 | 1.9 | 1710.6 | 1.3 | 5.0 | 2.3 | 0.7 | 1710.9 | 2.3 | 4.7 | 4.4 | 0.7 |
| WAG-H5-2#2508 | JF018 | −1690.7 | 3 | −1692.3 | 1.5 | 1.6 | 3.35 | 0.2 | −1692.2 | 2.5 | 1.5 | 6.5 | 0.2 |
| | JF020 | −1671.4 | 3 | −1673.1 | 2.9 | 1.7 | 4.15 | 0.1 | 1673.4 | 4.6 | 2.0 | 7.6 | 0.2 |
| | JFCD0906 | 1665.6 | 3 | 1664.0 | 1.3 | 1.6 | 3.25 | 0.2 | 1663.9 | 2.3 | 1.8 | 6.4 | 0.2 |
| | JFCD0912 | 1711.2 | 3 | 1710.6 | 1.3 | 0.6 | 3.25 | 0.1 | 1710.9 | 2.3 | 0.2 | 6.4 | 0.0 |

iGrav#067, we conducted continuous relative observations using CG-6#052 at a site adjacent to site JF018 (Figure 4). Figure 8 shows the Allan deviation of the residual gravity signals. The sensitivity was 16.2 μGal/Hz$^{1/2}$ at site JF018. A resolution of 1.8 μGal was obtained in 88 s, and 0.7 μGal was achieved in 1408 s.

The sensitivity of the WAG-H5-2#2508 gravimeter was first evaluated by a statistical time series analysis in comparison with the other gravimeters. One-second series were used for the

**Table 9.** Gravity difference ($\delta g$) before and after adjustment.

| Start site–end site | $\delta g$ (μGal) | $u_{\delta g}$ ($k$ = 1) (μGal) | $\delta\hat{g}$ (μGal) | $u_{\delta\hat{g}}$ ($k$ = 1) (μGal) | $\delta g - \delta\hat{g}$ (μGal) | $u_{\delta g - \delta\hat{g}}$ ($k$ = 1) (μGal) | $E_n$ |
|---|---|---|---|---|---|---|---|
| JF009–JF018 | 2.8 | 3.4 | 2.6 | 1.8 | 0.2 | 3.8 | 0.0 |
| JF018–JF020 | 17.8 | 3.0 | 18.8 | 2.6 | 1.0 | 4.0 | 0.1 |
| JF009–JFCD0912 | 3410.9 | 4.1 | 3405.7 | 1.7 | 5.2 | 4.4 | 0.4 |
| JFCD0912–JFCD0906 | −47.8 | 2.1 | −47.0 | 1.7 | −0.8 | 2.6 | 0.1 |

**Table 10.** Comparison reference values determined by all the absolute gravimeters.

| Site | Solution A | | Solution B | | Difference in CRVs (μGal) |
|---|---|---|---|---|---|
| | CRV (μGal) | $U_{1.10\text{m}}$ ($k$ = 2) (μGal) | CRV (μGal) | $U_{1.10\text{m}}$ ($k$ = 2) (μGal) | |
| JF009 | −1694.6 | 2.6 | −1694.8 | 2.4 | 0.2 |
| JF018 | −1692.3 | 2.9 | −1692.2 | 2.5 | −0.1 |
| JF020 | −1673.1 | 5.7 | −1673.4 | 4.6 | 0.3 |
| JFCD0906 | 1664.0 | 2.5 | 1663.8 | 2.3 | 0.2 |
| JFCD0912 | 1710.6 | 2.6 | 1710.9 | 2.3 | −0.3 |

**Table 11.** Degrees of equivalence of all the gravimeters corresponding to the CRVs in Table 6.

| Gravimeter | Solution A | | Solution B | |
|---|---|---|---|---|
| | DoE (μGal) | $U_i$ ($k$ = 2) (μGal) | DoE (μGal) | $U_i$ ($k$ = 2) (μGal) |
| A10#046 | 6.1 | 17.4 | 6.1 | 16.4 |
| FG5X#257 | −0.5 | 3.0 | −0.4 | 2.8 |
| FG5X#260 | −4.3 | 2.8 | −4.3 | 2.6 |
| A10#028 | 1.5 | 17.4 | 1.5 | 16.3 |
| FG5X#262 | 3.3 | 2.7 | 3.3 | 2.6 |
| FG5X#255 | −1.5 | 2.7 | −1.5 | 2.6 |
| IGG-03B#005 | 1.3 | 8.2 | 1.3 | 7.7 |
| FG5X#264 | 2.0 | 2.8 | 2.0 | 2.6 |
| WAG-H5-2#2508 | 1.4 | 5.0 | 1.4 | 4.6 |

iGrav#067, 88-s data for the WAG-H5-2#2508, 15-s data for the CG-6#052, and 10-s data for both the FG5X#257 and IGG-03B#005. The Allan standard deviations were calculated as shown in Figure 9. Analysis of the Allan standard deviations showed that the iGrav#067 demonstrated the highest sensitivity, followed by CG-6#052, WAG-H5-2#2508, FG5X#257, and IGG-03B#005. At an integration interval of 1000 s, the sensitivity of the IGG-03B#005 reached a level close to 1.0 μGal, and both the FG5X#257 and WAG-H5-2#2508 reached a level better than 1.0 μGal. At an integration interval of 60 s, the sensitivity of the CG-6#052 reached a level better than 1.0 μGal, and the iGrav#067 reached a level better than 0.1 μGal. All five instruments showed an increase over a long time period, likely because of environmental noise and tide residuals (Cook et al., 2021).

### 4.2 Precision and Repeatability

During the comparison, five absolute gravity measurements were conducted at the JF020 site between February 2 and February 6, 2026, by the WAG-H5-2#2508. The $g$-value at the instrument height of each day, based on 24-h averages with a sampling interval of half an hour, are shown in Figure 10. Note that the precision of $g$-values in the five measurements is better than 0.4 μGal. Figure 11 shows the distribution of the five $g$-values and its average with a standard deviation of 1.5 μGal. The standard deviation can be seen as a small time-scale repeatability for repeated measurements at the same site and orientation after restarting the instrument.

### 4.3 Long-Term Gravity Monitoring

At a fixed site, the complicated change in gravity with time is mainly caused by the tidal force, and a practical gravimeter should be able to carry out long-term gravity monitoring. Our WAG-H5-2#2508 gravimeter was transported from Wuhan to Tianjin and was operated consecutively over approximately 15 d, with a sampling interval of 88 s to test the long-term stability. The measured data have been corrected for theoretical values (Dehant et al., 1999), atmospheric pressure, polar motion, and the ocean

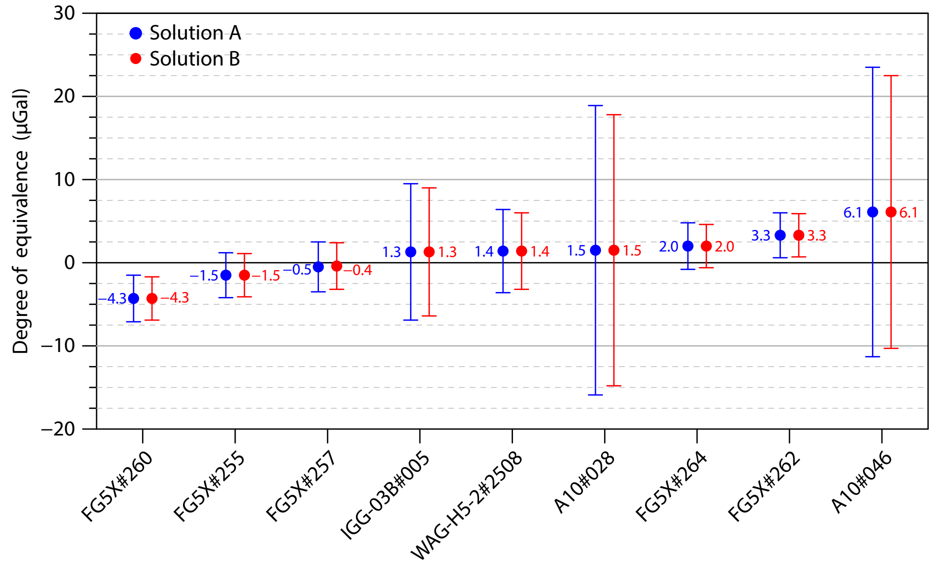


**Figure 7**. Degrees of equivalence of all the gravimeters. The error bars represent the instrumental expanded uncertainty ($U_i$) at a 95% confidence level corresponding to Table 11.

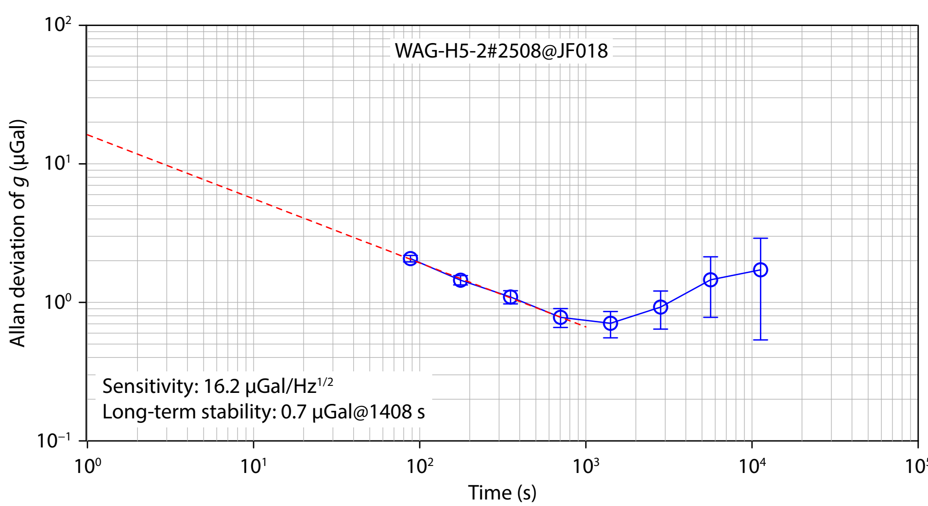


**Figure 8**. The standard Allan deviation at site JF018.

loading effect (Matsumoto et al., 2001). The continuous data are shown in Figure 12a, and the residuals of the experimental data are shown in Figure 12b. Note that the measured $g$-value is very consistent with the theoretical tidal model, and the residual is within 10 μGal at a sampling interval of 88 s.

## 5. Conclusions and Prospective

In this article, we present a comprehensive performance evaluation of the WAG-H5-2#2508 atom gravimeter, an upgraded second-generation transportable quantum gravimeter developed by CAS Cold Atom Technology (Wuhan) Co. Ltd. To rigorously evaluate the performance of the instrument, the WAG-H5-2#2508 participated in a 2026 absolute gravimeter comparison organized by the CMONOC project in Wuhan, China, alongside eight other absolute gravimeters. The comparison adopted a rigorous data processing framework: quadratic polynomial fitting was used to determine the precise VGG at each measurement site, superconducting gravimeter observations were used to unify all measurements to a common epoch, and two constrained least-squares adjustment solutions (Solution A with only absolute gravity data, Solution B combining absolute and relative gravity data) were implemented to derive CRVs and DoEs for each instrument. The comparison results demonstrated that all nine participating gravimeters showed good consistency, with DoEs ranging from −4.3 to 6.1 μGal at a 95% confidence level, indicating the long-term stability of absolute gravimeters. For the WAG-H5-2#2508, the DoE was 1.4 μGal with an expanded uncertainty of 5.0 μGal ($k$ = 2), and all measured $g$-values at four sites agreed well with the CRVs, with deviations between 0.2 and 2.0 μGal, confirming the high accuracy of the instrument.

A further performance analysis based on the comparison and long-term test data showed that the short-term sensitivity of WAG-H5-2#2508 reached 16.2 μGal/Hz$^{1/2}$, and the measurement precision achieved better than 1.0 μGal at an integration time of 1000 s,

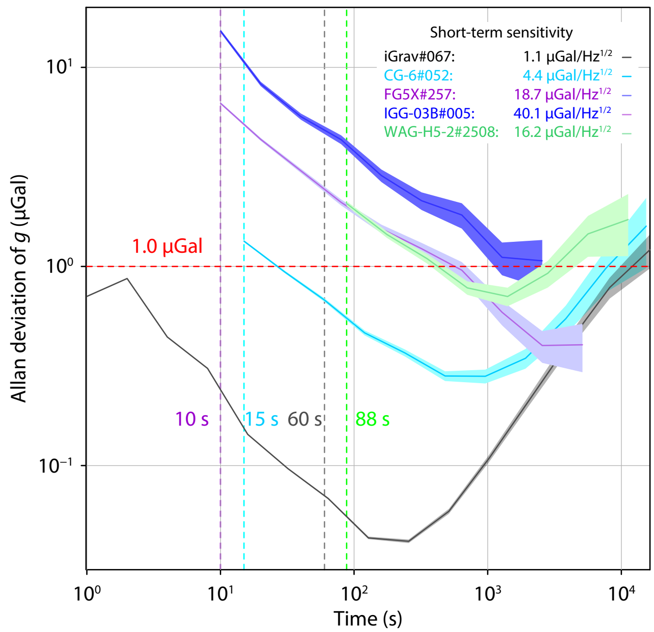


**Figure 9**. Standard Allan deviations of different types of gravimeters. The horizontal dashed red line shows the sensitivity benchmark of 1.0 μGal; the vertical dashed colored lines signify a sampling interval of 10 s for the FG5X#257 and IGG-03B#005 gravimeters, a sampling interval of 15 s for the CG-6#052 gravimeter, and a sampling interval of 88 s for the WAG-H5-2#2508 gravimeter; and the dashed black line signifies the integration period of 60 s.

approaching the sensitivity level of the FG5X, demonstrating performance comparable to the state of the art. Repeated 24-h measurements at the same site after instrument restart showed a daily measurement precision better than 0.4 μGal, and the repeatability of five independent measurements was 1.5 μGal, indicating excellent short-term and medium-term repeatability. A 15-d continuous gravity monitoring test with an 88-s sampling interval at another site showed that the residual after tidal and environmental corrections remained within 10 μGal, verifying the long-term stability and continuous operation capability of the instrument.

Atom gravimeters based on atom interferometry offer new measurement capabilities by combining high sensitivities and accuracies of a few microgal with the possibility of performing continuous measurements. Being absolute gravimeters, their scale factor is accurately determined and does not need calibration (Merlet et al., 2021). This is essential for application in the frame of fundamental metrology and offers a new realization of the kilogram in the revised International System of Units. As absolute gravimeters, they are expected to play a role in the quest for the establishment of a local, regional, and global absolute gravity reference system and frame (Wziontek et al., 2021). At present, the majority of gravity surveys utilize spring-based gravimeters, as they are significantly more compact and mobile. Spring-based gravimeters can attain similar levels of precision as atom gravimeters. For example, the CG6 gravimeter can attain a precision of 5 μGal after an integration time of 3 min in "quiet" environments (Francis, 2021; Li ZY and Hu MZ, 2026). However, spring-based gravimeters are relative instruments and are designed to have a reference *g*-value calibrated manually. Unfortunately, because of temperature dependencies within the hardware, mechanical wear and tear, and aging, the reference *g*-value drifts over time (zero drift). To circumvent zero drifts, the reference *g*-values need to be recalibrated regularly (Shettell et al., 2024). Hybrid gravimetry is the joint use of spring-based gravimeters with instruments providing gravity changes at the base sites, to determine the absolute changes at all sites of the network (Hector et al., 2015). It relies on the simultaneous use of different types of gravimeters: superconducting, absolute, or spring-based relative gravimeters (Hinderer et al., 2016). By combining atom absolute gravimeters with spring-based relative gravimeters, we can average the respective strengths of each technology while compensating for the limited mobility of atom absolute gravimeters and the poor long-term stability of spring-based gravimeters. In this combined approach, atom absolute gravimeters are used to obtain temporal gravity changes at one or several base sites, and relative gravity surveys provide spatial gravity differences relative to these base sites.

The scale factor of a superconducting gravimeter is usually calibrated by using simultaneous and colocated gravity measurements with the FG5 absolute gravimeter (Chen XD et al., 2013; Jia JG et al., 2015; Mu LS et al., 2019). The scale factor of the superconducting gravimeter is determined by applying a least-squares method to the parallel observation of superconducting gravimeter and absolute gravimeter data. The factors that limit the calibration precision are the precision of the absolute gravimeter and the amount of observation data (Xing LL et al., 2010). Because atom gravimeters have become a promising tool for ultra-high-precision measurements of absolute gravity, when calibrating the superconducting gravimeter using an atom gravimeter, its most prominent advantage is that there is no mechanical friction between atoms and the vacuum chamber during the drops of the test mass in an atom gravimeter system, compared with the FG5X absolute gravimeter. The mechanical dissipation in the FG5X absolute gravimeter would reduce the lifetime of the instrument. Therefore, atom gravimeters will be more suitable for continuous and long-term absolute gravity measurements in the future (Wang QY et al., 2018; Merlet et al., 2021).

The Earth's gravitational field and its variations represent a complex geophysical effect that requires joint instrumental observations based on diverse principles and methods. Currently, gravity measurement is mainly divided into three categories: the first uses superconducting gravimeters (SGs), the second uses absolute gravimeters (AGs), and the third uses spring-based relative gravimeters (RGs). The future development trend lies in the comprehensive observation and fusion of multi-method data, which is referred to as 3G hybrid gravimetry (SG + AG + RG; Wang JP et al., 2025). This approach integrates the three types of gravity observations into a continuous absolute observation network, enabling the generation of multi-source real-time gravity change maps. In 3G hybrid gravimetry, absolute gravity measurement

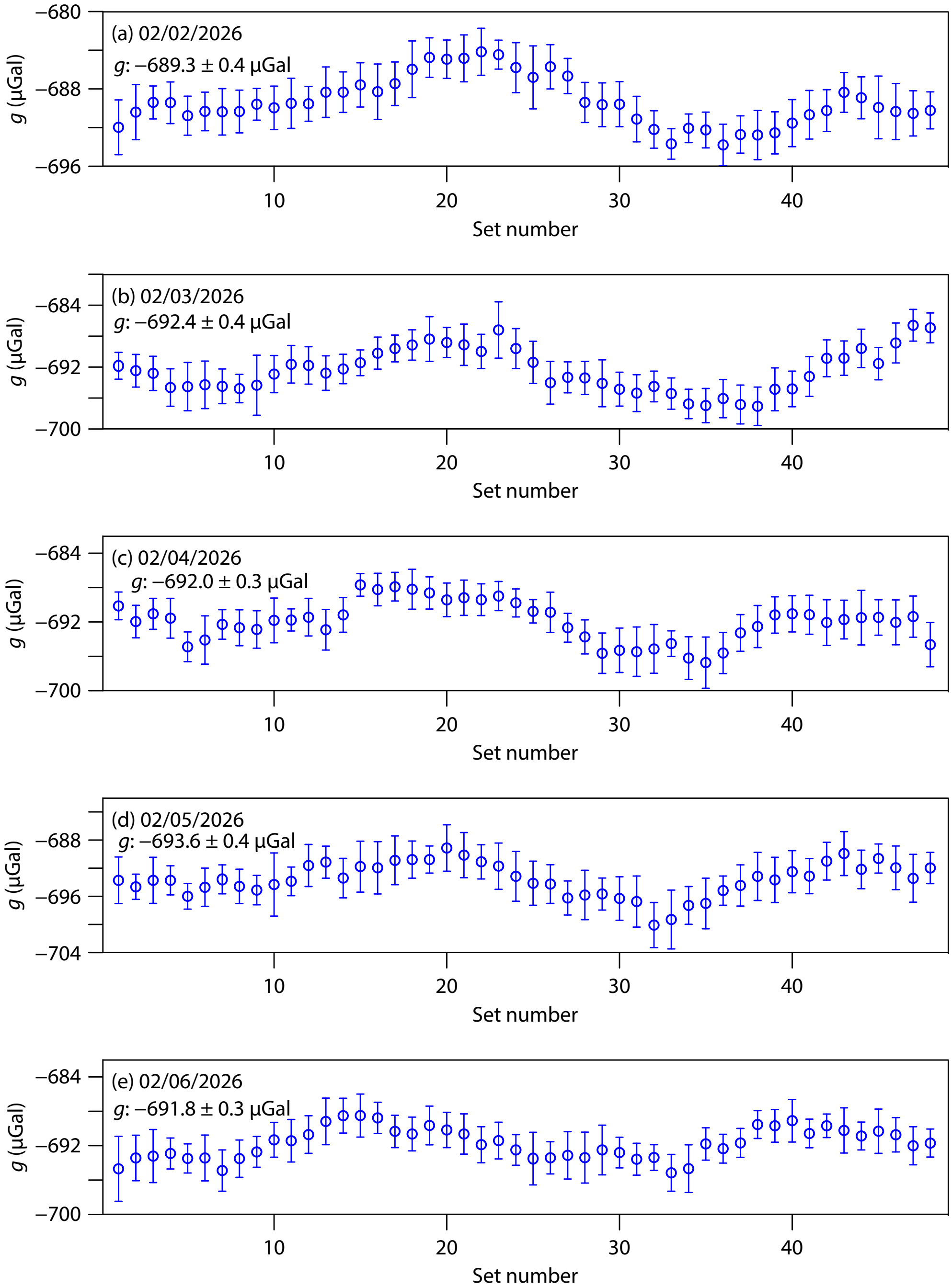


**Figure 10**. Results of five $g$-values and their precision at site JF020. The constant $g_0$ has been subtracted from the $g$-value. Each observation involved restarting the instrument. A single observation lasted continuously for 24 h, and a set $g$-value was obtained every half hour. The mean $g$-value and its precision were calculated based on the total number of sets.

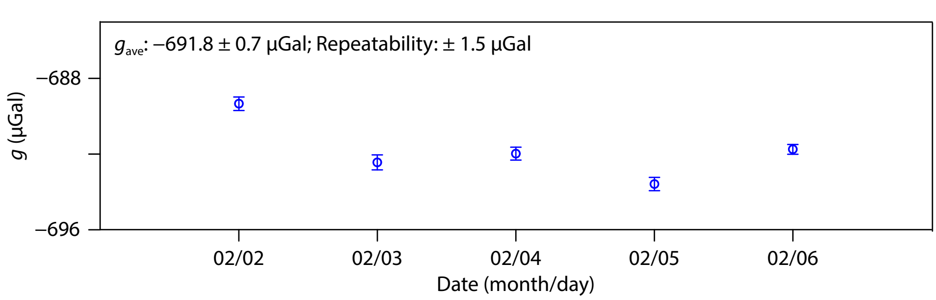


**Figure 11**. Results of the average and standard deviation of the five $g$-values (from Figure 10).

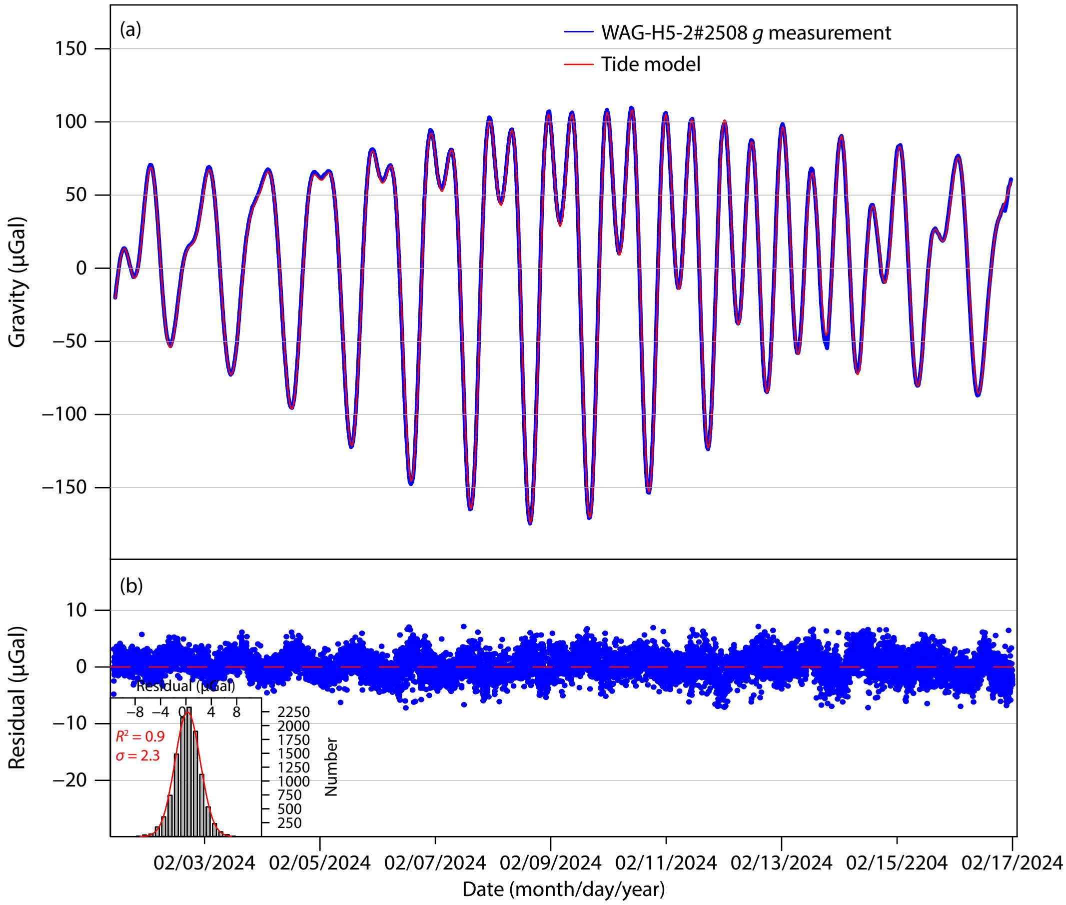


**Figure 12**. Results of long-term experimental data. (a) Tide data measured from February 1 to 16, 2024. The blue line represents the experimental data, and the red line is the theoretical tidal model. (b) Residual.

plays a core role: it provides reference benchmarks for spring-based relative gravimeters, calibrates the scale factors of superconducting gravimeters, and corrects their zero drift. Therefore, absolute gravity measurement will continue to play an irreplaceable key role in future 3G hybrid gravimetry.

## Acknowledgments

We thank Chunjian Li of the National Institute of Metrology for her discussion on the comparison data processing. This work was supported by the National Key Research and Development Program of China (Grant No. 2023YFF0713505-4), the Natural Science Foundation of Wuhan (Grant No. 2024040801020247), and the National Science and Technology Major Project for Deep Earth Probe and Mineral Resources Exploration (Grant No. 2024ZD1002700).

## References

Chen, X. D., Sun, H. P., Zhang, W. M., and Hao, X. H. (2013). Accuracy analysis on determination of calibration factor of a superconducting gravimeter using an absolute gravimeter. *J. Geod. Geodyn. (in Chinese)*, *33*(5), 145–149. https://doi.org/10.14075/j.jgg.2013.05.008

Cook, A. K., Champollion, C., and Le Moigne, N. (2021). First evaluation of an absolute quantum gravimeter (AQG#B01) for future field experiments. *Geosci. Instrum. Mehod. Data Syst.*, *10*(1), 65–79. https://doi.org/10.5194/gi-10-65-2021

Crossley, D., Hinderer, J., and Riccardi, U. (2013). The measurement of surface gravity. *Rep. Prog. Phys.*, *76*(4), 046101. https://doi.org/10.1088/0034-4885/76/4/046101

Dehant, V., Defraigne, P., and Wahr, J. M. (1999). Tides for a convective Earth. *J. Geophys. Res.: Solid Earth*, *104*(B1), 1035–1058. https://doi.org/10.1029/1998JB900051

Fang, J., Wang, W. Z., Zhou, Y., Li, J. T., Zhang, D. F., Tang, B., Zhong, J. Q., Hu, J. G., Zhou, F., … Zhan, M. S. (2024). Classical and atomic gravimetry. *Remote Sens.*, *16*(14), 2634. https://doi.org/10.3390/rs16142634

Feng, J. Y., Wu, S. Q., Li, C. J., Wang, Q. Y., Mu, L. S., and Su, D. W. (2022). International comparison method of absolute gravimeter. *Rev. Geophys. Planet. Phys. (in Chinese)*, *53*(3), 269–277. https://doi.org/10.19975/j.dqyxx.2021-059

Francis, O. (2021). Performance assessment of the relative gravimeter Scintrex CG-6. *J. Geod.*, *95*(10), 116. https://doi.org/10.1007/s00190-021-01572-y

Guo, D. M., Chen, X. D., Xue, Z. X., He, H. Y., Xing, L. L., Ma, X., and Niu, X. W. (2023). High-accuracy quasi-geoid determination using Molodensky's series solutions and integrated gravity/GNSS/leveling data. *Remote Sens.*, *15*(22), 5411. https://doi.org/10.3390/rs15225414

Hector, B., Séguis, L., Hinderer, J., Cohard, J. M., Wubda, M., Descloitres, M., Benarrosh, N., and Boy, J. P. (2015). Water storage changes as a marker for base flow generation processes in a tropical humid basement catchment (Benin): Insights from hybrid gravimetry. *Water Resour. Res.*, *51*(10), 8331–8361. https:// https://doi.org/10.1002/2014WR015773

Hinderer, J., Hector, B., Mémin, A., and Calvo, M. (2016). Hybrid gravimetry as a tool to monitor surface and underground mass changes. In J. T. Freymueller, et al. (Eds.), *Proceedings of the IAG General Assembly: International Symposium on Earth and Environmental Sciences for Future Generations* (pp. 123–130). Prague, Czech Republic: Springer. https://doi.org/10.1007/1345_2016_253

Huang, P. W., Tang, B., Chen, X., Zhong, J. Q., Xiong, Z. Y., Zhou, L., Wang, J., and Zhan, M. S. (2019). Accuracy and stability evaluation of the $^{85}$Rb atom gravimeter WAG-H5-1 at the 2017 International Comparison of Absolute Gravimeters. *Metrologia*, *56*(4), 045012. https://doi.org/10.1088/1681-7575/ab2f01

Jia, J. G., Luan, W., and Shen, W. B. (2015). Accurate determination of the calibration factor of iGrav-007 superconducting gravimeter. *Geomat. Inform. Sci. Wuhan Univ. (in Chinese)*, *40*(10), 1366–1370,1376. https://doi.org/10.13202/j.whugis20130780

Jiang, Z., Pálinkáš, V., Francis, O., Jousset, P., Mäkinen, J., Merlet, S., Becker, M., Coulomb, A., Kessler-Schulz, K. U., … Lequin, D. (2012). Relative gravity measurement campaign during the 8th International Comparison of Absolute Gravimeters (2009). *Metrologia*, *49*(1), 95–107. https://doi.org/10.1088/0026-1394/49/1/014

Li, C. J., Wu, S. Q., Su, D. W., Feng, J. Y., Choi, I. M., Kim, M. S., Mou, L. S., Wang, Q. Y., Hu, R., … Zhang, W. M. (2022). Result analysis of the first Asia-Pacific comparison of absolute gravimeters. *MAPAN*, *37*(3), 553–564. https://doi.org/10.1007/s12647-022-00570-5

Li, C. Y., Long, J. B., Huang, M. Q., Chen, B., Yang, Y. M., Jiang, X., Xiang, C. F., Ma, Z. L., He, D. Q., … Chen, S. (2023). Continuous gravity measurement with a portable atom gravimeter. *Phys. Rev. A*, *108*(3), 032811. https://doi.org/10.1103/PhysRevA.108.032811

Li, Z. C., Zhang, P., and He, Z. T. (2018). Construction of the national gravity datum points and accuracy assessment. *Geomat. World (in Chinese)*, *25*(1), 55–58,64. https://doi.org/10.3969/j.issn.1672-1586.2018.01.012

Li, Z. Y., and Hu, M. Z. (2026). Static drift characteristics of CG6 relative gravimeter. *J. Geod. Geodyn. (in Chinese)*, *46*(2), 184–188. https://doi.org/10.14075/j.jgg.2025.02.048

Matsumoto, K., Sato, T., Takanezawa, T., and Ooe, M. (2001). GOTIC2: A program for computation of oceanic tidal loading effect. *J. Geod. Soc. Jpn.*, *47*(1), 243–248. https://doi.org/10.11366/sokuchi1954.47.243

Merlet, S., Gillot, P., Cheng, B., Karcher, R., Imanaliev, A., Timmen, L., and dos Santos, F. P. (2021). Calibration of a superconducting gravimeter with an absolute atom gravimeter. *J. Geod.*, *95*(5), 62. https://doi.org/10.1007/s00190-021-01516-6

Mu, L. S., Feng, J. Y., Wang, Q. Y., Li, C. J., Wu, S. Q., and Sun, B. (2019). Analysis of calibration factor of superconducting gravimeter iGrav-012. *Acta Metrol. Sin*. (in Chinese), *40*(3), 373–377. https://doi.org/10.3969/j.issn.1000-1158.2019.03.04

Sánchez, L., Wziontek, H., Wang, Y. M., Vergos, G., and Timmen, L. (2023). Towards an integrated global geodetic reference frame: Preface to the special issue on reference systems in physical geodesy. *J. Geod.*, *97*(6), 59. https://doi.org/10.1007/s00190-023-01758-6

Shettell, N., Lee, K. S., Oon, F. E., Maksimova, E., Hufnagel, C., Wei, S. J., and Dumke, R. (2024). Geophysical survey based on hybrid gravimetry using relative measurements and an atomic gravimeter as an absolute reference. *Sci. Rep.*, *14*, 6511. https://doi.org/10.1038/s41598-024-57253-1

Sun, H. P., Zhang, H. K., Xu, J. Q., Chen, X. D., Zhou, J. C., and Zhang, M. M. (2019). Influences of the Tibetan plateau on tidal gravity detected by using SGs at Lhasa, Lijiang and Wuhan stations in China. *Terr. Atmos. Ocean. Sci.*, *30*(1), 139–149. https://doi.org/10.3319/TAO.2019.02.14.01

Sun, W. K., Wang, Q., Li, H., Wang, Y., Okubo, S., Shao, D. S., Liu, D. Z., and Fu, G. Y. (2009). Gravity and GPS measurements reveal mass loss beneath the Tibetan Plateau: Geodetic evidence of increasing crustal thickness. *Geophys. Res. Lett.*, *36*(2), L02303. https://doi.org/10.1029/2008GL036512

Tian, W., Zhang, W. M., Xue, H. P., and Zhong, M. (2022). Components test review of the miniaturized absolute gravimeter IGG-03B. *J. Huazhong Univ. Sci. Technol. (Nat. Sci. Ed.) (in Chinese)*, *50*(9), 30–34. https://doi.org/10.13245/j.hust.220905

Timmen, L. (2003). Precise definition of the effective measurement height of free-fall absolute gravimeters. *Metrologia*, *40*(2), 62–65. https://doi.org/10.1088/0026-1394/40/2/310

Van Camp, M., de Viron, O., Watlet, A., Meurers, B., Francis, O., and Caudron, C. (2017). Geophysics from terrestrial time-variable gravity measurements. *Rev. Geophys.*, *55*(4), 938–992. https://doi.org/10.1002/2017RG000566

Wang, J. P., Han, Y. F., Zhang, X. L., Li, Z. Y., Zhang, M. H., Zhu, J., Yang, G. L., Hu, M. Z., and Shen, C. Y. (2025). Application and research progress of absolute gravity observation in China. *Rev. Geophys. Planet. Phys. (in Chinese)*, *56*(3), 243–257. https://doi.org/10.19975/j.dqyxx.2024-022

Wang, L. S., Chen, C., Kaban, M. K., Du, J. S., Liang, Q., and Thomas, M. (2014). The use of the A10-022 absolute gravimeter to construct the relative gravimeter calibration baselines in China. *Metrologia*, *51*(3), 203–211. https://doi.org/10.1088/0026-1394/51/3/203

Wang, Q. Y., Feng, J. Y., Wang, S. K., Zhuang, W., Zhao, Y., Mou, L. S., and Wu, S. Q. (2018). Calibration of the superconducting gravimeter based on a cold atom absolute gravimeter at NIM. *Chin. Phys. B*, *27*(12), 123701. https://doi.org/10.1088/1674-1056/27/12/123701

Wang, S. H. (2021). *Error Theory and Surveying Adjustment* (3rd ed.) (in Chinese). Shanghai: Tongji University Press.

Wang, S. K., Zhao, Y., Zhuang, W., Li, T. C., Wu, S. Q., Feng, J. Y., and Li, C. J. (2018). Shift evaluation of the atomic gravimeter NIM-AGRb-1 and its comparison with FG5X. *Metrologia*, *55*(3), 360–365. https://doi.org/10.1088/1681-7575/aab637

Wu, S. Q., Feng, J. Y., Li, C. J., Su, D. W., Wang, Q. Y., Hu, R., and Mou, L. S. (2021). The results of 10th International Comparison of Absolute Gravimeters (ICAG-2017). *J. Geod.*, *95*(6), 63. https://doi.org/10.1007/s00190-021-01517-5

Wziontek, H., Bonvalot, S., Falk, R., Gabalda, G., Mäkinen, J., Pálinkáš, V., Rülke, A., and Vitushkin, L. (2021). Status of the international gravity reference system and frame. *J. Geod.*, *95*(1), 7. https://doi.org/10.1007/s00190-020-01438-9

Xing, L. L., Li, H., Liu, Z. W., Xuan, S. B., and Hao, H. T. (2010). Scale factor calibration of a superconducting gravimeter by using absolute gravimetry. *J. Geod. Geodyn. (in Chinese)*, *30*(1), 48–50. https://doi.org/10.14075/j.jgg.2010.01.001

Xu, A. P., Kong, D. L., Fu, Z. J., Wang, Z. Y., and Lin, Q. (2019). Vibration compensation of an atom gravimeter. *Chin. Opt. Lett.*, *17*(7), 070201. https://doi.org/10.3788/COL201917.070201

Xu, G. C. (2010). *Sciences of Geodesy-I: Advances and Future Directions*. Berlin: Springer. https://doi.org/10.1007/978-3-642-11741-1

Xu, Y. Y., Cui, J. F., Qi, K., Chen, L. L., Deng, X. B., Luo, Q., Zhang, H., Tan, Y. J., Shao, C. G., … Hu, Z. K. (2022). Evaluation of the transportable atom gravimeter HUST-QG. *Metrologia*, *59*(5), 055001. https://doi.org/10.1088/1681-7575/ac8258

Xue, G. Q., Zhou, N. N., Su, B. X., Zhang, A. K., Yang, Y. C., Mo, J. P., and Wu, X. (2024). Geophysical exploration strategy for Cu-Ni-Co deposits in China: A review. *Geophysics*, *89*(1), WB25–WB34. https://doi.org/10.1190/geo2023-0034.1

Zhou, M. K., Duan, X. C., Chen, L. L., Luo, Q., Xu, Y. Y., and Hu, Z. K. (2015). Micro-Gal level gravity measurements with cold atom interferometry. *Chin. Phys. B*, *24*(5), 050401. https://doi.org/10.1088/1674-1056/24/5/050401

Zhu, H. R., Huang, P. W., Gao, B., Tang, B., Chen, X., Zhong, J. Q., Wang, J., and Zhan, M. S. (2024). Miniaturized optical system for high-precision mobile atomic gravimeters. *Opt. Express*, *32*(15), 26157–26166. https://doi.org/10.1364/OE.528832